Genomic Consequences of and Demographic Response to Pervasive Hybridization Over Time in Climate-Sensitive Pikas

Deyan Ge,[1,†] Zhixin Wen,[1,†] Anderson Feijó,[1,†] Andrey Lissovsky,[2,†] Wei Zhang,[3,†] Jilong Cheng,[1] Chaochao Yan,[4] Huishang She,[1] Dezhi Zhang,[1] Yalin Cheng,[1] Liang Lu,[5] Xinlai Wu,[6] Danping Mu,[7] Yubo Zhang,[3] Lin Xia,[1] Yanhua Qu,[1] Alfried P. Vogler,[8,9] and Qisen Yang*,[1]

[1]Key Laboratory of Zoological Systematics and Evolution, Institute of Zoology, Chinese Academy of Sciences, Beijing, 100101, China

[2]Severtsov Institute of Ecology and Evolution RAS, Leninskiy pr. 33, Moscow,119071, Russia

[3]State Key Laboratory for Protein and Plant Gene Research, Peking-Tsinghua Center for Life Sciences at College of Life Sciences, Peking University, Beijing, 100871, China

[4]CAS Key Laboratory of Mountain Ecological Restoration and Bioresource Utilization & Ecological Restoration and Biodiversity Conservation Key Laboratory of Sichuan Province, Chengdu Institute of Biology, Chinese Academy of Sciences, Chengdu, 610041, China

[5]State Key Laboratory for Infectious Diseases Prevention and Control, National Institute for Communicable Disease Control and Prevention, Chinese Center for Disease Control and Prevention, Beijing, 102206, China

[6]The Key Laboratory of Zoological Systematics and Application, School of Life Science, Institute of Life Science and Green Development, Hebei University, Baoding, 071002, China

[7]Xinjiang Key Laboratory of Biological Resources and Genetic Engineering, College of Life Science and Technology, Xinjiang University, Urumqi, 830046, China

[8]Department of Life Sciences, Natural History Museum, London, SW7 5BD, UK

[9]Department of Life Sciences, Imperial College London, Silwood Park Campus, Ascot, SL5 7PY, UK

[†]These authors contributed equally to this work.

***Corresponding author:** E-mail: quyh@ioz.ac.cn;a.vogler@imperial.ac.uk; yangqs@ioz.ac.cn.

Associate editor: Bing Su

Abstract

Rare and geographically restricted species may be vulnerable to genetic effects from inbreeding depression in small populations or from genetic swamping through hybridization with common species, but a third possibility is that selective gene flow can restore fitness (genetic rescue). Climate-sensitive pikas (*Ochotona* spp.) of the Qinghai–Tibetan Plateau (QHTP) and its vicinity have been reduced to residual populations through the movement of climatic zones during the Pleistocene and recent anthropogenic disturbance, whereas the plateau pika (*O. curzoniae*) remains common. Population-level whole-genome sequencing ($n = 142$) of six closely related species in the subgenus *Ochotona* revealed several phases of ancient introgression, lineage replacement, and bidirectional introgression. The strength of gene flow was the greatest from the dominant *O. curzoniae* to ecologically distinct species in areas peripheral to the QHTP. Genetic analyses were consistent with environmental reconstructions of past population movements. Recurrent periods of introgression throughout the Pleistocene revealed an increase in genetic variation at first but subsequent loss of genetic variation in later phases. Enhanced dispersion of introgressed genomic regions apparently contributed to demographic recovery in three peripheral species that underwent range shifts following climate oscillations on the QHTP, although it failed to drive recovery of northeastern *O. dauurica* and geographically isolated *O. sikimaria*. Our findings highlight differences in timescale and environmental background to determine the consequence of hybridization and the unique role of the QHTP in conserving key evolutionary processes of sky island species.

Key words: **phylogenomics, adaptive introgression, hybridization, speciation, Lagomorpha.**

Article

Introduction

"Genetic rescue" and "genetic swamping" represent the double-edged sword of hybridization in driving the diversification and adaptation of isolated, small populations, and rare species. Under the first hypothesis, hybridization is a mechanism that introduces genetic variation into local populations affected by inbreeding (rescue), which subsequently may catalyze diversification and sympatric speciation (Litsios and Salamin 2014; Stelkens et al. 2014; Whiteley et al. 2015; Grant and Grant 2019). Introgressed elements may be identified as fixed alleles in the genome of a recipient population and may play important roles in local adaptation (Duranton et al. 2020; Owens and

Samuk 2020; Pulido-Santacruz et al. 2020; Myers et al. 2021). Adaptive traits in advanced-generation hybrids surpass the parental phenotypic range, a phenomenon known as heterosis (in F1) or transgressive segregation (heritably stable) (Cevik et al. 2019). Allowing gene flow into isolated populations or rare species is thus considered a promising strategy to alleviate genetic load and decrease the extinction risk of isolated populations (Frankham 2015). Under the second hypothesis, hybridization reduces diversity through the breakdown of reproductive barriers and then drives rare species to extinction as local genotypes are replaced in the hybrids (Vuillaume et al. 2015; Quilodran et al. 2020; Kottler et al. 2021). Meanwhile, population growth rates may be reduced due to hybrid incompatibility or outbreeding depression (Moyle and Nakazato 2010; Feng et al. 2019; Moerman et al. 2020; Kottler et al. 2021). Hybridization is a widely recognized process limiting the range expansion of narrow-ranged species (Mark and Barton 1997; Kottler et al. 2021). The conflicting outcomes from either hypothesis raise outstanding questions for conservation planning and evolutionary biology. Notably, what are the exact genomic consequences of hybridization for the decline of small-ranged species as the genetic load becomes high, and how can hybridization contribute to the recovery and persistence of recipients after they experience a demographic decline?

A key aspect in studying the above processes is the time since hybridization (Waller 2015; Bell et al. 2019). Human activities have caused habitat fragmentation and population decline for thousands of species (Dirzo et al. 2014), prompting a call to consider genetic rescue in conservation (Ralls et al. 2018), for example, by allowing pulses of gene flow from distant lineages to restore small, isolated populations of rare species in wildlife conservation (Fitzpatrick et al. 2016; Weeks et al. 2017; Ralls et al. 2020). Studies of domesticated animals and crops have shown that heterosis is usually only evident for 1–3 generations after hybridization (Goulet et al. 2017; Labroo et al. 2021), and the evolutionary outcomes and demographic responses to inbreeding depression are detectable in hybrids within a few generations (Johnson et al. 2011; Ceballos et al. 2018). In contrast, outbreeding depression may not manifest until the occurrence of temporary heterosis and additional genomic incompatibilities resulting from recombination and then largely outside the timeframe of monitoring and conservation activities (Fenster and Galloway 2000). Thus, investigations of the fate of introgressed genomic regions and their precise role in determining novel traits are needed. This could be achieved by studying hybridization events that occurred over different periods in nature and reflect the evolutionary processes of selection, genetic diversification, and ecological trait changes over time in the recipient species under different environmental conditions.

Extant pikas (genus *Ochotona*, see fig. 1) are a relict group of Lagomorpha (hares, rabbits, and pikas) that were highly diversified in the early to middle Miocene but have experienced dramatic levels of species extinction, local extirpation, and range contraction since the late Miocene (Grayson 2005; Ge et al. 2012, 2013; Arregoitia et al. 2015). They are now mainly confined to the alpine region on the Qinghai–Tibetan Plateau (QHTP), with fragmented distributions in Central and northern Asia and North America (Lissovsky 2016; Melo-Ferreira and Alves 2018; Smith et al. 2018). Notably, pikas are cold-tolerant yet highly sensitive to environmental changes and thus have been considered sentinels for climate change and keystone species of high-altitude ecosystems (Smith and Foggin 1999; Galbreath et al. 2009; Lanier et al. 2015; Smith et al. 2019). Four pika species (*O. koslowi*, *O. argentata*, *O. iliensis*, and *O. hoffmanni*) are now ranked as endangered, and three others (*O. curzoniae*, *O. princeps*, and *O. pusilla*) are suffering population decline (Lissovsky 2016; Smith et al. 2018). Extant species of pikas are assigned to five subgenera: *Lagotona* (Kretzoi, 1941), *Alienauroa* (Liu et al. 2017), *Conothoa* (Lyon, 1904), *Pika* (Lacépède, 1799), and *Ochotona* (Link, 1795; Liu et al. 2017). The last is different from the other four in surrounding the QHTP, with *O. dauurica* extending to the north of China, Mongolia and Russia (fig. 1A) and assigned as the QHTP group (Niu et al. 2004) or the shrub-steppe group (Wang, Liang, et al. 2020). Several species in the subgenus *Ochotona* that are the target of this study (*O. nubrica*, *O. sikimaria*, and *O. thomasi*) have very limited geographic ranges, rendering them vulnerable, whereas *O. curzoniae* is widespread in the QHTP; despite its recent decline, it is considered a pest (Delibes-Mateos et al. 2011; Wilson and Smith 2015). These species showed distinct ecological differentiation; for example, *O. thibetana* prefers alpine forests in the Hengduan Mountains, *O. cansus* prefers alpine bushes and is slightly higher than O. *thibetana* in elevational distribution, *O. thomasi* inhabits alpine shrubs in the northeast of QHTP, *O. dauurica* is distributed in open meadows on top of mountains in the northeastern QHTP and central China and extends to grasslands in Mongolia and southern Russia, *O. curzoniae* occupies the widest range on the plateau surface of QHTP, and *O. sikimaria* is confined to a small region that borders China and India in southeast QHTP. Previous studies dated the divergence time of the subgenus *Ochotona* to the late Miocene, approximately 6 Mya (Ge et al. 2012, 2013; Wang, Liang, et al. 2020). Phylogenetic analyses have already identified widespread incongruence among nuclear and mitochondrial markers in this subgenus, raising the possibility of gene flow from the widespread *O. curzoniae* to other species (Koju et al. 2017; Castillo Vardaro et al. 2018; Lissovsky et al. 2019). The prominent incongruence of mitochondrial markers with morphological species boundaries has been mainly investigated in the context of taxonomic questions (Liu et al. 2017; Lissovsky et al. 2019; Wang, Liang, et al. 2020) but also offers opportunities to investigate the consequences of genomic introgression at different time points during lineage evolution as well as their demographic dynamics following rapid anthropogenic changes.

In the present study, we integrated morphological, genomic, and ecological data to interpret the differentiation

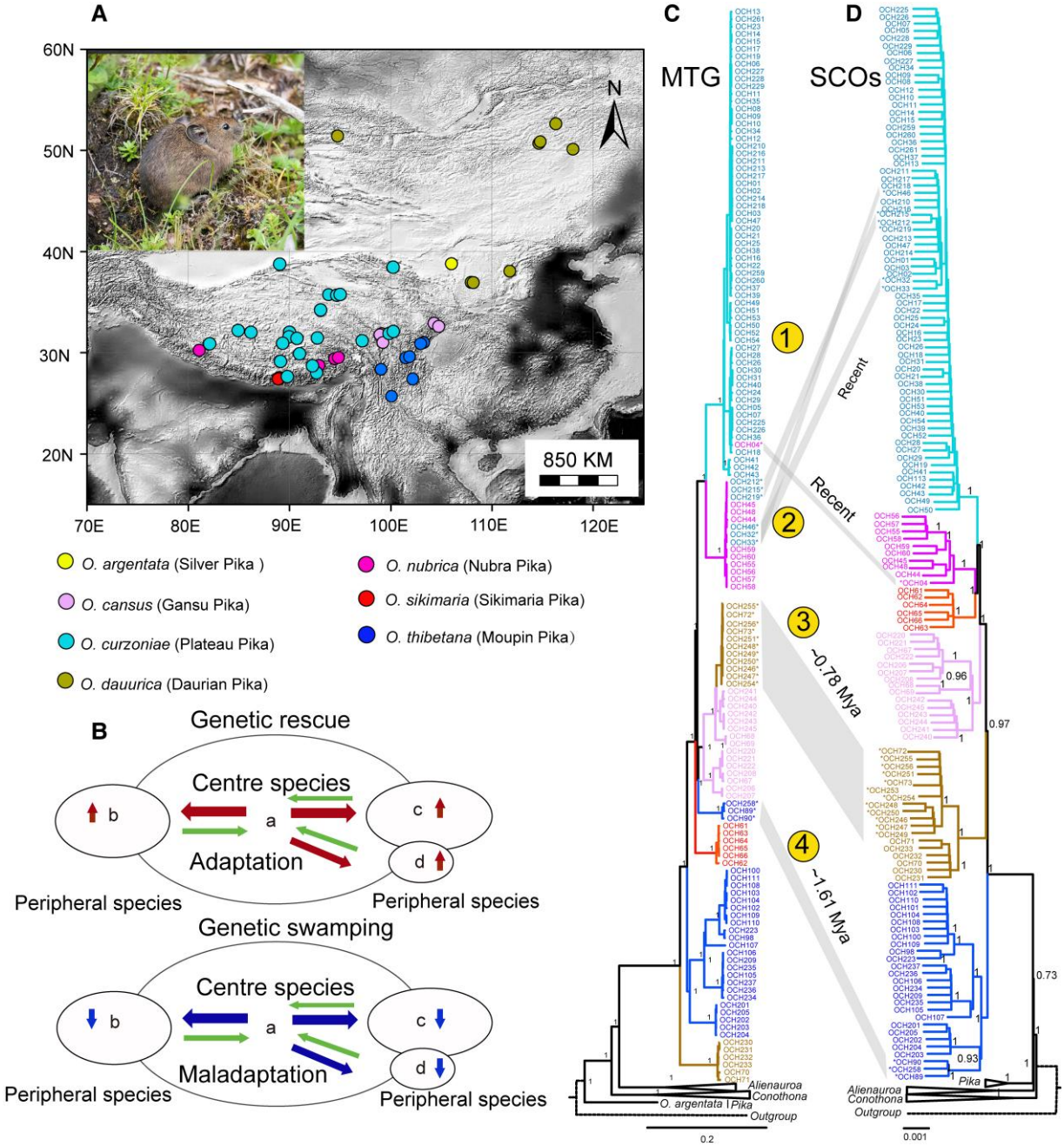

Fig. 1. (*A*) Habitus of *O. cansus* (photographed by Prof Xin Zhou in the Wanglang National Nature Reserve, Sichuan Province, China) and sample locations of molecular voucher specimens for whole-genome sequencing. (*B*) Two hypotheses on the genomic consequences of hybridization. "Genetic rescue" and "genetic swamping" refer to two hypotheses on the genomic consequences of hybridization in the subgenus *Ochotona*; arrows in the large center circles show asymmetric gene flow, and arrows in the small circles show demographic changes of narrow-ranged peripheral species. (*C*) Phylogenetic tree inferred from 13 protein-coding sequences of MTGs. (*D*) Phylogenetic tree from single-copy orthologs (SCOs). Four hypothetical mitochondrial introgression events are highlighted by links between the MTG and SCO trees and numbered 1, 2, 3, and 4.

and evolution of six closely related species in the subgenus *Ochotona*. The dominant plateau pika, *O. curzoniae* (the central species), inhabits most of the QHTP, whereas all others (the peripheral species) are distributed near the edge of the QHTP, and only *O. dauurica* extends to northern China, Mongolia, and Russia (fig. 1A). We first established that species pairs with mitonuclear incongruence also show clear signals of gene flow in nuclear genomes. Dating these introgressions established the order of discrete events of mitochondrial and nuclear gene exchange. We then tested the effects of gene flow from the center to the peripheral species, which either could result in the acquisition of beneficial alleles (genetic rescue) or the broad incompatibility of introgressed alleles and maladaptation, with opposing outcomes for the recipient populations following the hybridization event (fig. 1A). These processes

must be seen in the context of climatic oscillations affecting these populations that not only drive range contraction introducing local inbreeding but also determine the long-range movement permitting interspecific contact and then relieving the homozygosity burden of inbreeding (fig. 1*B*). Our study provides an integrative view of the adaptive features of introgression and the environmental conditions that facilitate interspecific gene flow in pika speciation, adaptive radiation, and demographic dynamics.

Results

Mitonuclear Discordance and Divergence Time

We first established the validity of the seven morphologically recognized species of the subgenus *Ochotona*. Geometric morphometric analyses of 191 cranium specimens (supplementary fig. S1*A*, Supplementary Material online and supplementary table S1, Supplementary Material online) showed overlaps in skull morphology, most prominently among *O. nubrica*, *O. thibetana*, and *O. sikimaria*, and between *O. curzoniae* and *O. dauurica*, both in dorsal and ventral views, in addition to distinct variation from their closest sister species *O. thomasi*. Analysis of variance (ANOVA) and pairwise comparison analyses revealed significant differences between most pairs of species ($P < 0.001$, supplementary tables S2 and S3, Supplementary Material online), but insignificant variations were identified between many species pairs, for example, *O. cansus* and *O. curzoniae*, *O. cansus* and *O. dauurica*, *O. nubrica* and *O. thibetana*, *O. thibetana* and *O. thomasi* in the overall size of the dorsal view. The principal component plots showed low overlap in the morphospace between species that showed mitonuclear discordances in phylogenetic reconstruction (fig. 1), especially in the dorsal view (supplementary fig. S1, *B* and *C*, Supplementary Material online).

To ensure that we used accurate species assignments in the following analyses, we sequenced the mitochondrial *CYTB* gene of 328 specimens sampled across their species ranges and analyzed them together with those available in GenBank ($n = 726$, supplementary table S4, Supplementary Material online). Moreover, we extracted the protein-coding regions of the mitochondrial genome (MTG) sequences created from the assemblies of shotgun reads ($n = 241$, supplementary tables S5 and S6, Supplementary Material online), and 115 of them were newly generated in this study. We also obtained single-copy orthologs (SCOs) of the nuclear genome (supplementary tables S5 and S6, Supplementary Material online), extracting between 1815 and 9166 complete SCO sequences for a total of 142 individuals.

Phylogenetic reconstruction using *CYTB* (supplementary fig. S2, Supplementary Material online) and whole MTGs equally revealed seven main clades, each of which broadly represented one of the morphologically assigned species. However, several specimens were not placed in the morphologically assigned species, suggesting mitochondrial introgression (fig. 1*C*). All sequences that nominated *O. yarlungensis* (KU359551–KU359561) were clustered in *O. nubrica*, which supports *O. yarlungensis* established by Liu et al. (2017) as a junior synonym of *O. nubrica* (Lissovsky et al. 2019). A species tree reconstructed from gene trees of 6710 SCOs (supplementary table S5, Supplementary Material online) in ASTRAL-III (Zhang et al. 2018) also recovered each of the six species of *Ochotona* as monophyletic, without showing the outliers detected in the MTG (fig. 1*D*).

The pairs of species of suspected mitonuclear discordance showed no intermediate variation in either dorsal or ventral view in the morphometric analysis, indicating the same distinct skulls as nonadmixed populations (supplementary fig. S1, Supplementary Material online). Based on incongruence with the SCOs and morphology, we recognize four cases of mitochondrial introgression due to the shift in the position of specific individuals, specifically 1) from *O. nubrica* to *O. curzoniae* (six individuals); 2) from *O. curzoniae* to *O. nubrica* (one individual); 3) from *O. cansus* to *O. dauurica* (11 individuals); and 4) a sublineage of *O. thibetana* that formed a distinct monophyletic lineage branching off at the base of the *O. cansus* to the *O. curzoniae* clade (three individuals) (fig. 1*C* and *D*, supplementary fig. S3, supplementary table S7, Supplementary Material online). The latter corresponds to a "ghost" clade from Qionglai Mountain (fig. 1*C* and *D*) that in a previous study was assigned to an extinct species only detected from haplotypes introgressed into *O. thibetana*. This lineage was clustered into the main clade of *O. thibetana* to form a sister lineage to samples from the Liang Mountains. Those from the northern Hengduan Mountains, Yunling Mountains, and Qionglai Mountains were clustered as another monophyletic sister clade (Ge et al. 2022). This pattern rejected the "ghost" clade being assigned as independent species, nominated as "*O. qionglaiensis*' by Liu et al. (2017). Principal component analysis using the whole-genome SNP data that were mapped to the genome of American pika (*O. princeps*, assembly OchPri4.0) (Sjodin et al. 2021) revealed a remarkable overlap among species, despiting a neighbor-joining tree that was supported by the monophyly of each species (fig. 2*A* and *B*).

Calibrations with SCOs to date these four waves of MTG introgression showed that 1) and 2) correspond to very recent, possibly ongoing bidirectional introgression between *O. curzoniae* and *O. nubrica* and vice versa (supplementary fig. S4, *A–D*, Supplementary Material online), whereas 3) corresponds to an ancient introgression from *O. cansus* to *O. dauurica* (supplementary fig. S5, *A–D*, Supplementary Material online) at 0.78 Mya (fig. 2*C*), and 4) represents introgression from some extinct species to *O. thibetana* (Ge et al. 2022) at 1.61 Mya. The split of *O. thibetana* from all others as the basal separation in the lineages affected by admixture was dated to 4.97 Mya, with the divergence of the remaining lineages in the subgenus *Ochotona* starting at approximately 4.63 Mya (fig. 2*C*). According to the distribution of MTG-admixed populations, three hybrid zones were identified (supplementary fig. S3*D*,

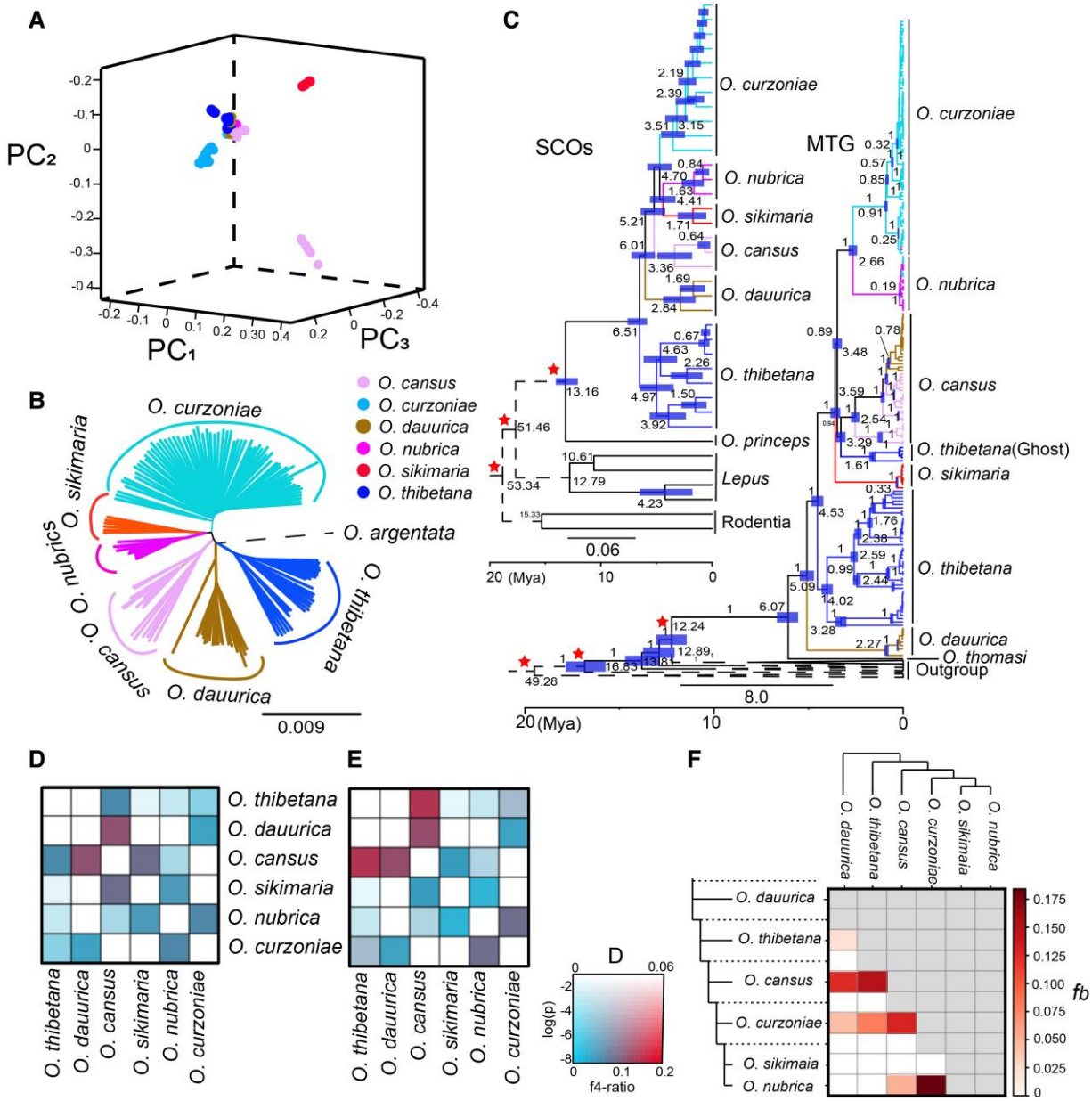

Fig. 2. Genetic structure and hybridization among species. (*A*) Genetic structure inferred using PCA. (*B*) A neighbor-joining tree was inferred using SNPs. (*C*) Divergence time inferred using the MTG and SCOs of the whole genome. (*D*) Gene flow detected by using ABBA–BABA statistics in Dsuite. (*E*) Gene flow determined using the F4-ratio. (*F*) Gene flow determined using the f-branch method.

Supplementary Material online): the current hybrid zone of *O. nubrica* and *O. curzoniae* located in the western Himalayas; the southeastern edge of the QHTP in northern Sichuan, southern Qionghai, and southwestern Qinlin, where *O. dauurica* hybridized with *O. cansus*; and a hypothetical hybrid zone in the western region of the Sichuan Basin in Qionglai Mountain, where *O. thibetana* hybridized with a presumably extinct species.

Overall Gene Flow Among Species in Nuclear Genomes and Accompanying Demographic Dynamics

We used four software programs to identify general trends of gene flow in the nuclear genome. First, we tested shared ancestry components among individuals of the six species using Admixture (Alexander and Lange 2011) under $K = 6–9$ ancestral groupings. Values of $K = 7$ gave the best match to the six species of *Ochotona* (supplementary fig. S6A, Supplementary Material online). Although separating these species, the method still showed apparent ancestry admixture in *O. cansus*, *O. thibetana*, and *O. curzoniae* but not in *O. dauurica*, *O. nubrica*, and *O. sikimara*, which only partly reflected the expectations from mitogenome introgression (supplementary fig. S6, *B* and *C*, Supplementary Material online).

Next, we used TreeMix (Pickrell and Pritchard 2012), a method that simultaneously builds population trees and tests for gene flow. A phylogenetic tree with migration

events from 0 to 5 was constructed. The number of migration events that best fit the data was identified as 3 (migration edge = 3). This analysis identified gene flow from *O. nubrica* to *O. curzoniae*, from O. *cansus* to *O. nubrica*, and from the ancestor of *O. curzoniae* and *O. cansus* to *O. dauurica* (supplementary fig. S7*A–F*, Supplementary Material online). Gene flow from *O. nubrica* to *O. curzoniae* was identified when the migration edge = 1, and gene flow from *O. cansus* to *O. dauurica* was displayed when the migration edge = 4. In addition, we identified a significant introgression signal between most species pairs using the ABBA–BABA statistic in Dsuite (Malinsky et al. 2021). A total of 15 of 20 comparisons produced *Z* scores >3, indicating high introgression, and the comparison of *O. cansus* and *O. dauurica* showed the strongest signal ($P < 0.001$, supplementary table S8, Supplementary Material online, fig. 2*D*). All 15 comparisons were supported by admixture proportions above 5% in the f_4-ratio measure. Moreover, we also identified strong gene flow between *O. cansus* and *O. thibetana* and *O. cansus* and *O. dauurica* with the f_4-ratio test (fig. 2*E*) and strong gene flow between *O. nubrica* and *O. curzoniae*, *O. cansus* and *O. dauurica*, and *O. cansus* and *O. curzoniae* in the f-branch method (fig. 2*F*). This method can disentangle correlated f_4-ratio results and assign gene flow evidence to specific internal branches on the phylogeny (Malinsky et al. 2018).

G-PhoCS (Gronau et al. 2011) is different from the methods above in its ability to infer ancestral population sizes, population divergence times, and migration rates from genome sequences at the same time. Here, a coalescent model implemented in G-PhoCS revealed migration among the six species (fig. 3*A*), with the highest levels occurring from *O. curzoniae* to *O. thibetana* (4.03%) and from *O. curzoniae* to *O. dauurica* (2.44%). G-PhoCS identified *O. curzoniae* as having the largest population size among the examined species (fig. 3*B*), and gene flow from this species distributed in the central plateau to the species with distribution at lower altitudes at the periphery of the plateau was greater than that in the opposite direction (fig. 3*A*). This result was consistent with that of the f-branch method, which identified strong gene flow between the center (*O. curzoniae*) and peripheral species (*O. nubrica*, *O. cansus*, *O. thibetana*, and *O. dauurica*).

Demographic dynamics were inferred using the pairwise and multiple sequentially Markovian coalescent (PSMC) (Li and Durbin 2011), the latter implemented in SMC++ (Terhorst et al. 2017), inferring fluctuations in effective population size by linking the origin of heterozygous sites in a genome to a molecular clock (Gronau et al. 2011). The PSMC (Li and Durbin 2011) model identified two periods of population size increase in *O. curzoniae* and *O. nubrica* but only one peak in *O. sikimaria* from approximately 1 million to 10 thousand years ago, with the population sizes of these species decreasing overall (supplementary fig. S8, Supplementary Material online). Distinct demographic dynamics were found for different sublineages in *O. cansus*, *O. thibetana*, and *O. dauurica*, in which admixed populations in *O. dauurica* and *O. thibetana* deviated from nonadmixed populations to form two peaks, indicating that gene flow events influenced the demographic dynamics in these species. The results of SMC++, which is based on multiple genomes providing greater resolution and an extended time frame, also identified the long-term decline of all species, albeit in cyclical population size variation in the last ten thousand years (fig. 3*C*). In addition, a surprising trend of population size increase in four species was found in the last six thousand years; meanwhile, only *O. dauurica* continued to decline, and *O. sikimaria* increased slightly near the present after a dramatic decrease from its peak in the last seven thousand years (fig. 3*C*).

Local Ancestry Inference of Admixed Populations

In an effort to identify the genomic localization of introgressed segments in admixed populations (fig. 4), we performed local ancestry analysis (LAI) implemented in Loter (Dias-Alves et al. 2018), which determines the admixed portions as a mosaic of segments inherited from two ancestors. For this analysis, populations of *O. curzoniae* and *O. dauurica* from different sample localities ($n > 3$) were assigned to groups to test the strength of gene flow (see fig. 1 and supplementary Table S8, Supplementary Material online). Both the *D* and f_4-ratio values identified significant gene flow ($P < 0.001$) between *O. curzoniae* from Cuona (CN, fig. 5*A*) and Pulan (PL), where mitochondrial admixture is occurring, and *O. nubrica*, whereas those from Anduo (AND), Gaize (GZ), and Yadong (YD) were insignificant ($P > 0.05$, supplementary fig. S9, Supplementary Material online). The strength of gene flow between *O. dauurica* from Shaanxi and Shanxi of China (CH, fig. 5*B*) and *O. cansus* was greater than that of *O. dauurica* from Russia (RU, supplementary fig. S9, Supplementary Material online).

Moreover, we tested the phylogenetic relationships that vary across the genome using population genomic data due to both variations in lineage sorting and introgression in Twisst (Martin and Belleghem 2017). The proportion of *O. curzoniae* from CN clustered with *O. nubrica* was slightly higher than that of other populations (3.1% vs. 2.6–2.7%), and the proportion of *O. dauurica* from CH clustered within *O. cansus* was slightly higher than that from RU (1% vs. 0.5%). Here, a higher proportion implies a higher probability of interspecific genomic introgression (supplementary fig. S10, Supplementary Material online). Based on these results and mitonuclear discordance in phylogenetic reconstruction, we assigned populations of *O. curzoniae* from CN and PL as representatives of admixed populations (AD), whereas that of AND was representative of nonadmixed population (NO). Populations of *O. dauurica* from CH were assigned as admixed populations (AD), whereas populations of *O. dauurica* from RU were assigned as nonadmixed populations (NO).

Starting with *O. nubrica* and admixed populations of *O. curzoniae* (hybridization event "1" in fig. 1) from CN and PL, we found that 380,571 (0.25%) and 159,890 (1%) of the 14,959,431 SNP sites suffered introgression. None of

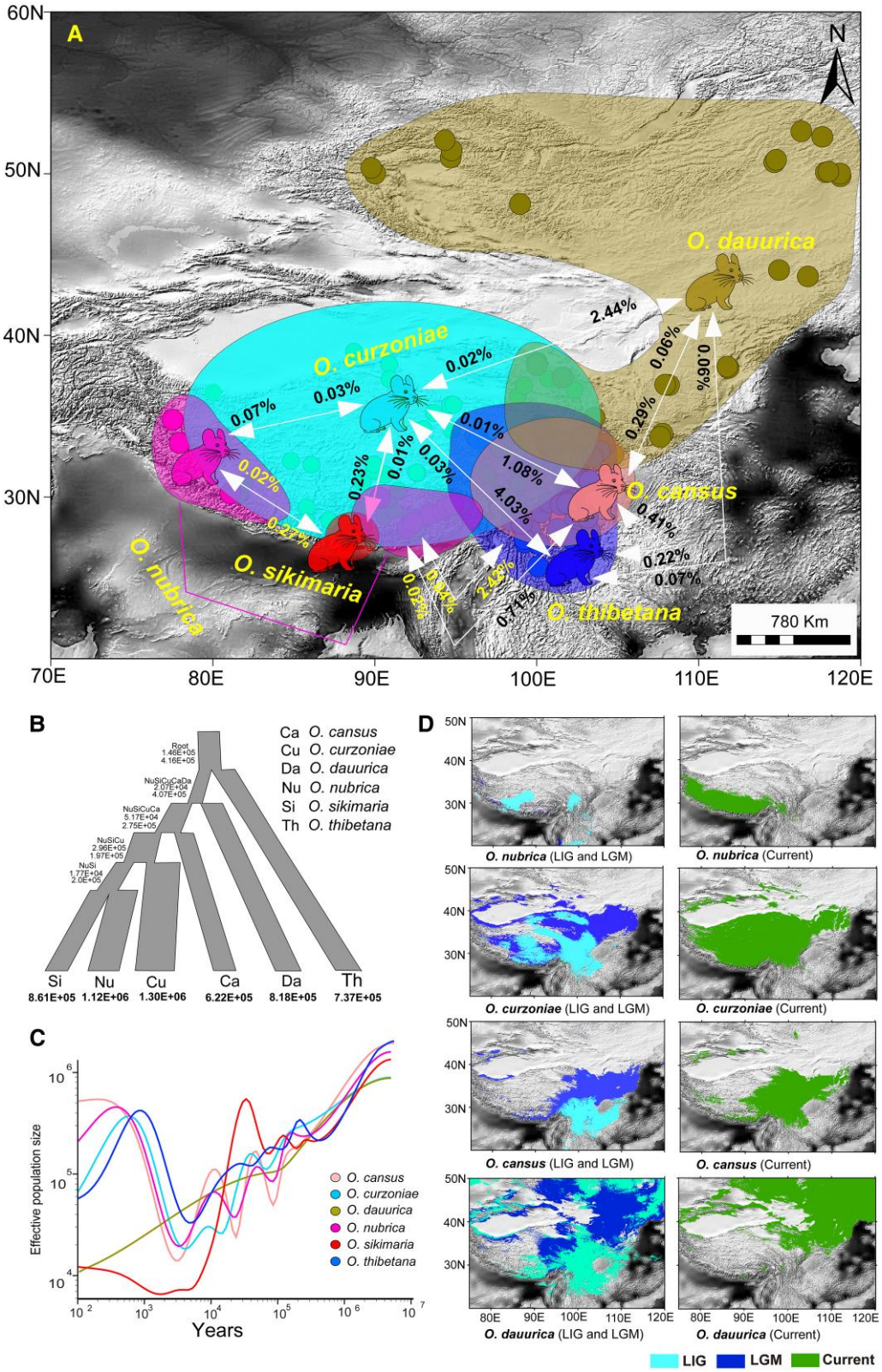

Fig. 3. Gene flow among species, demographic history of target species, and range shift of two major species pairs. (*A*, *B*). Effective population size and direction and strength of gene flow detected using G-PHoCS. (*C*) Demographic dynamics were inferred using SMC++. (*D*) Range shift of species that showed mitochondrial introgression in different historical periods (*O. curzoniae* and *O. nubrica* during early hybridization and *O. cansus* and *O. dauurica* after ancient introgression). Note the distribution of *O. curzoniae* on the central plateau region not occupied by the other species.

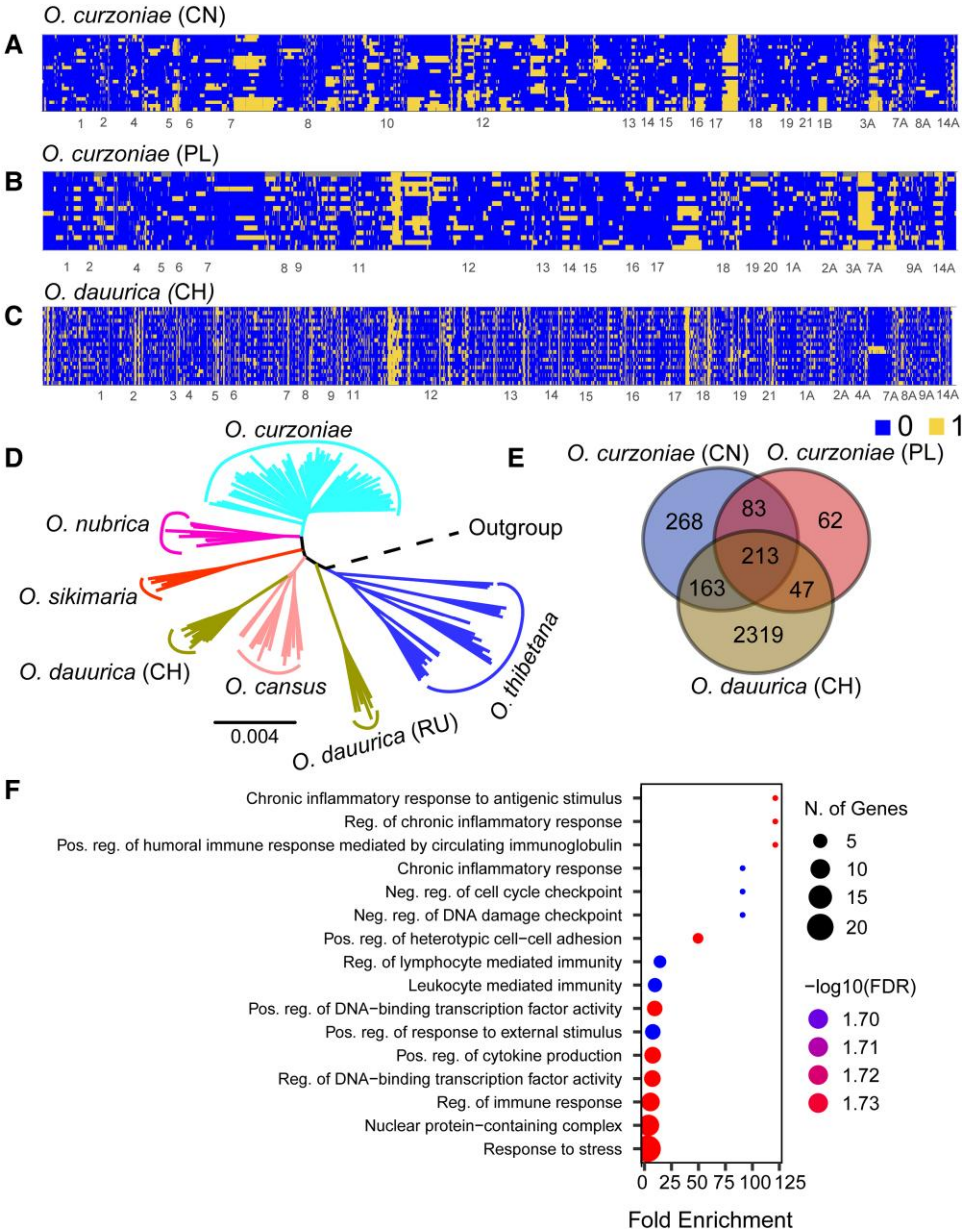

Fig. 4. Local ancestry inference of admixed populations of *O. curzoniae* and *O. dauurica* and functional annotation of introgressed genes. (*A*, *B*) Local ancestry inference for *O. curzoniae* from Cuona (CN) and Pulan (PL), which are undergoing genomic introgression from *O. nubrica*. (*C*) Local ancestry inference for *O. dauurica* from Shanxi and Shannxi in China (CH), which experienced ancient introgression from *O. cansus*. SNPs absence of introgression was deleted in A–C. (*D*) A neighbor-joining tree of all fixed introgression sites that were identified in *O. dauurica*. (*E*) A Venn diagram showing introgressed genes in *O. curzoniae* and *O. dauurica*. (*F*) GO analyses of the shared introgressed genes in *O. curzoniae* and *O. dauurica*. Fold enrichment is defined as the percentage of genes in the list belonging to a pathway divided by the corresponding percentage in the background (Ge et al. 2020).

these sites was fixed in the admixed populations (fig. 4*A* and *B*). In this analysis, nonadmixed *O. curzoniae* and *O. nubrica* were used as two sources for the admixed *O. curzoniae*. In the *O. dauurica*–*O. cansus* pair, a total of 1,260,881 introgressed sites were identified among a total of 14,959,431 sites (8.42%) admixed in *O. dauurica* from CH, among which 35,390 sites (0.2%) were fixed in all individuals (fig. 4*C*). In this analysis, nonadmixed *O. dauurica* and *O. cansus* were presumed to be the sources for the admixed *O. dauurica*. Annotation of these segments revealed that 97 genes were located in the fixed regions, represented as "1" in all admixed individuals (fig. 4*C*, supplementary table S9, Supplementary Material online). This was in contrast to the situation in *O. curzoniae*, which did not show the fixation of any introgressed site (fig. 4*A*). A phylogenetic analysis based on these fixed sites in *O. dauurica* placed admixed populations of *O. dauurica* in a cluster within *O. cansus* (fig. 4*C*), which mirrored the phylogenetic pattern presented in the MTG tree (hybridization event 3 in fig. 1*C*).

Annotation of introgressed elements revealed 727 genes in *O. curzoniae* from CN, 405 genes in *O. curzoniae* from PL, and 2,742 genes in admixed *O. dauurica* that had experienced introgression (fig. 4*A*–*C*). Generally, introgressed segments in *O. curzoniae* are longer segments than in *O. dauurica* (i.e., in the presumed older hybridization event) (fig. 4*A*). The LAIs in admixed and nonadmixed pairs of *O. curzoniae* and *O. dauurica* revealed a total of 213 genes common to both sets of *O. curzoniae* and *O. dauurica* (fig. 4*D*). GO enrichment analyses (fig. 4*E*, supplementary table S10 and S11, Supplementary Material online) linked their functions to the response to stress, nuclear protein-containing response, immunity and so on using American pika as the background species (88 of 213 genes were mapped to the background species) and to immune response, regulation of DNA-binding transcription factor activity, immune

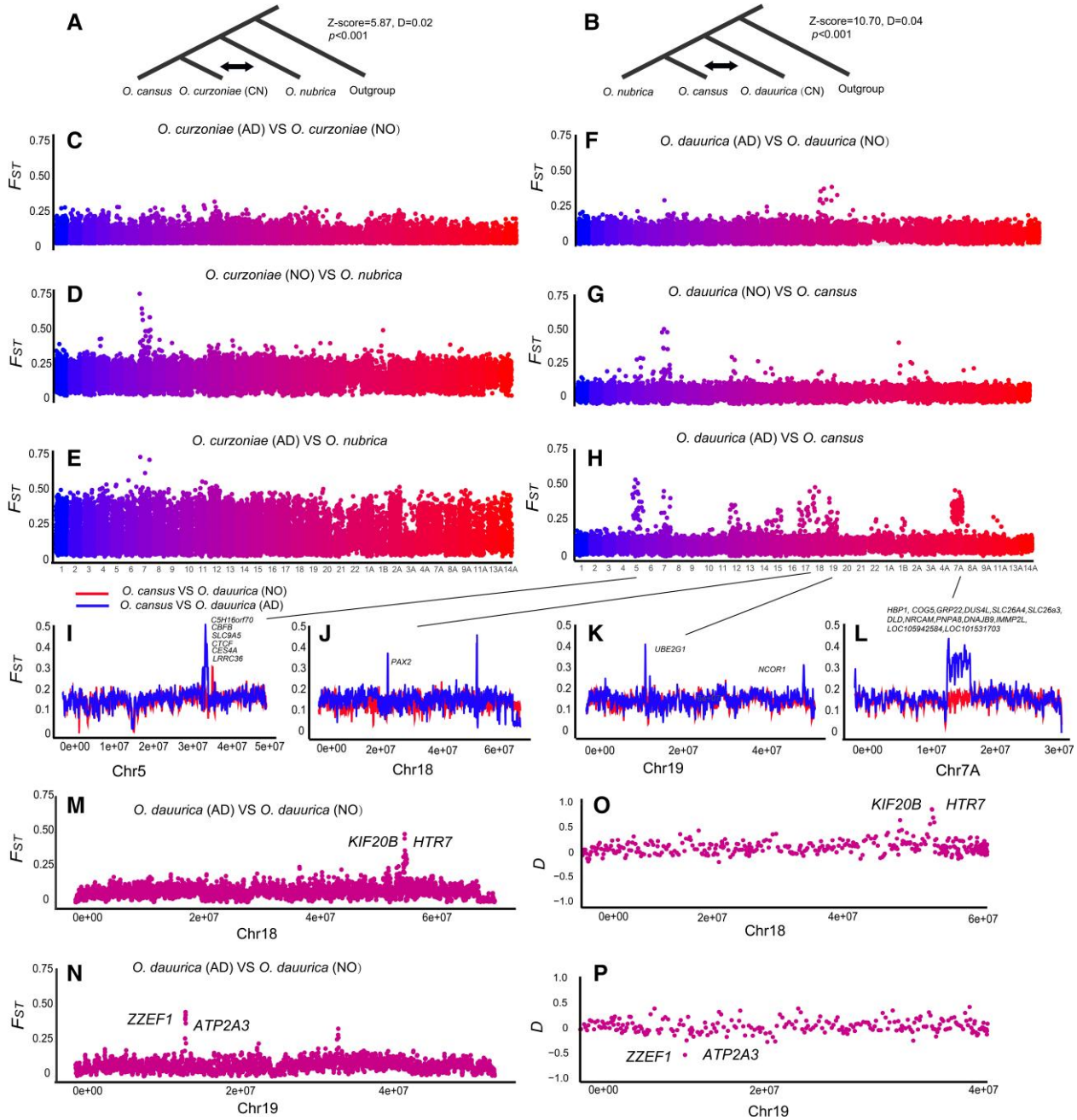

Fig. 5. (*A*, *B*) The ABBA–BABA test identified significant gene flow between *O. curzoniae* and *O. nubrica* and between *O. casus* and *O. dauurica*. (*C*) *FST* test of admixed population *O. curzoniae* from Cuona (AD) versus nonadmixed *O. curzoniae* from Anduo (NO). (*D*) *FST* test of *O. nubrica* versus nonadmixed *O. curzoniae* from Anduo (NO). (*E*) *FST* test of *O. nubrica* versus introgressed *O. curzoniae* from Cuona (AD), with sympatric distributions. (*F*) Admixed *FST* test of *O. dauurica* from Shaanxi and Shanxi in China (AD) versus nonadmixed *O. dauurica* from Russia (NO). (*G*) *FST* test of *O. cansus* versus nonadmixed *O. dauurica* from Russia (NO). (*H*) *FST* test of *O. cansus* versus admixed *O. dauurica* from Shanxi and Shaanxi (AD). (*I*–*L*) Details of chromosomes 5, 7A, 18, and 19 in panel H. (*M*, *N*). Details of chromosomes 18 and 19 in panel F. (*O*, *P*) Details of chromosomes 18 and 19 in the ABBA–BABA test.

response-regulating signal pathway and so on using the mouse as the background species (146 of 213 genes were mapped to the background species). The function of fixed genes in O. *dauurica* using the Americas pika as the background species (42 of 97 genes were mapped to the background species) was related to small molecular binding, nucleotide binding, nucleoside phosphate binding, anion binding, and so on (supplementary figs. S12 and S13, Supplementary Materials online); meanwhile, when we used the mouse as the background species (79 of 97 genes were mapped to the background species), the significantly enriched biological pathways were related to the negative regulation of ion transport, cation transport, mental ion transport, DNA damage checkpoint, calcium transport and calcium ion homeostasis (supplementary tables S8 and S9, Supplementary Material online).

"Genomic Slands of Differentiation" Between Admixed, Nonadmixed Populations and Donors

The overall F_{ST} values were prominently elevated both in admixed *O. curzoniae* and *O. dauurica* (tested with their donor species) when compared with that of nonadmixed populations (fig. 5*C*–*H*). However, in contrast to the presumed recently introgressed genomes of *O. curzoniae*, the increased F_{ST} in *O. dauurica* was limited to a few small outlier regions, which were absent between nonadmixed populations. Notably, F_{ST} outliers in several regions between sympatric admixed *O. dauurica* and *O. cansus* (fig. 5*I*–*L*) included a large highly divergent block of approximately 0.6 Mb on chromosome 7A (fig. 5*L*), which showed a higher value of linkage disequilibrium (supplementary fig. S14, Supplementary Material online). GO enrichment analyses revealed that genes in this region are mainly related to the maintenance of intracellular physiology and sperm capacitation (supplementary table S14, Supplementary Material online). *SLC26A3* and *DLD*, two key genes related to spermatogenesis, spermatid development, and sperm capacitation, are located in this region. Results in Loter indicated these *FST* outliers mainly resulted from genomic introgression (supplementary table S15, Supplementary Material online). This was further evidenced by the increase of local topological weightings that clustered the admixed *O. dauurica* from China with *O. cansus* using sliding windows on chromosome 7A (supplementary fig. S16, Supplementary Material online). Moreover, two further outlier regions that were identified as introgressed elements as well as outliers to distinguish admixed and nonadmixed lineages in *O. dauurica*, *HTR7* and *ATP2A3*, were located on chromosomes 18 and 19, respectively (fig. 5*M*–*P*). Phylogenetic analysis placed the copies from admixed lineages of *O. dauurica* together with those from *O. cansus*, the presumed donor (supplementary fig. S11, Supplementary Material online).

Genome Genetic Load and Inbreeding Depression Strengthened Under Harsh Environmental Changes

Genetic load (Bertorelle et al. 2022) and runs of homozygosity (ROH) (Ceballos et al. 2018) have been widely used to estimate the decrease in fitness due to outbreeding or inbreeding depression. We compared the genetic load of populations by measuring the genomic occurrence of synonymous/nonsynonymous mutations, frameshifts, and other loss-of-function mutations after whole-genome SNP variants were classed into different coding categories (Cingolani et al. 2012). Comparisons of three types of measures of genetic load (loss of function, LOF, missense genetic load, and synonymous genetic load) were generally higher in the admixed than nonadmixed populations in *O. dauurica* (ANOVA $P < 0.05$, fig. 6*A*–*C*) compared with the other five species ($P < 0.05$, fig. 6*D*–*F*). A comparison of the three parameters across the six species consistently revealed that the dominant *O. curzoniae* had the lowest genetic load (fig. 6*D*–*F*). Testing the genome level ROH (supplementary table S17, Supplementary Material online) as a useful indicator of homozygosity burden revealed that historically declining *O. sikimaria* and *O. dauurica* had a significantly larger number of short ROHs (>2 kb, fig. 6*G*) than the other species, whereas *O. nubrica* had a larger number of long ROHs (>200 kb, fig. 6*H*, supplementary fig. S17, Supplementary Material online). Here, longer ROHs are inherited from inbreeding of recent common ancestors, shorter ROHs are residual genomic signals of inbreeding in ancient history, and recombination events make the original long ROH short during evolution (Ceballos et al. 2018). Mapping the distribution of samples revealed *O. dauurica* locate in the region with a higher amplitude of temperature change from LIG to LGM and a higher level of human impact (fig. 6*I* and *J*).

Range Shifts in Different Historical Periods

Environmental niche models (ENMs) can be used to reconstruct historical range movements that may have affected the opportunities for hybridization at various time points since the last glacial maximum (LGM) and last interglacial (LIG). ENM identified range shifts in *O. cansus* southeast of the QHTP and *O. curzoniae* on the plateau surface from the LIG to the present conditions (fig. 3*D*), whereas *O. dauurica* experienced dramatic range contraction in the same period, being distributed in the area affected by the large temperature oscillation between the LIG and LGM of ∼5–8 °C (fig. 6*I*). As a result, the modern range of *O. dauurica* is largely nonoverlapping with *O. cansus*, that is the source of MTG introgression for *O. dauurica* (fig. 1*C*); meanwhile, historically, these species were codistributed in large parts of the eastern QHTP, which would have allowed hybridization (fig. 3*I*–*L*). In contrast, the ranges of *O. nubrica* that experienced distribution fragmentation at LGM (fig. 3*E*) expanded into the northwestern QHTP (fig. 3*F*), where it now overlaps with *O. curzoniae* (fig. 3*F* and *G*). Finally, the postglacial ranges are overlain by the recent impact of human activities affecting *O. dauurica* and *O. sikimaria* in particular (fig. 6*J*), consistent with a large population size decline starting approximately seven thousand years ago (fig. 3*D*).

Discussion

Different Methods for Detecting Genomic Introgression

Genome sequencing at the population level is improving our understanding of the role of hybridization in lineage evolution and speciation. Previous studies specifically focused on the question of population divergence in the presence of gene flow and the formation of "speciation islands" arising in the earliest stages of speciation (Wolf and Ellegren 2017; Papadopulos et al. 2019). As these studies can be extended across broader lineages that include several anciently separated species, a more complete picture of the historical effects of hybridization arises. Here, we used population-level samples across a small clade (six species) of the genus *Ochotona* to study the evolutionary

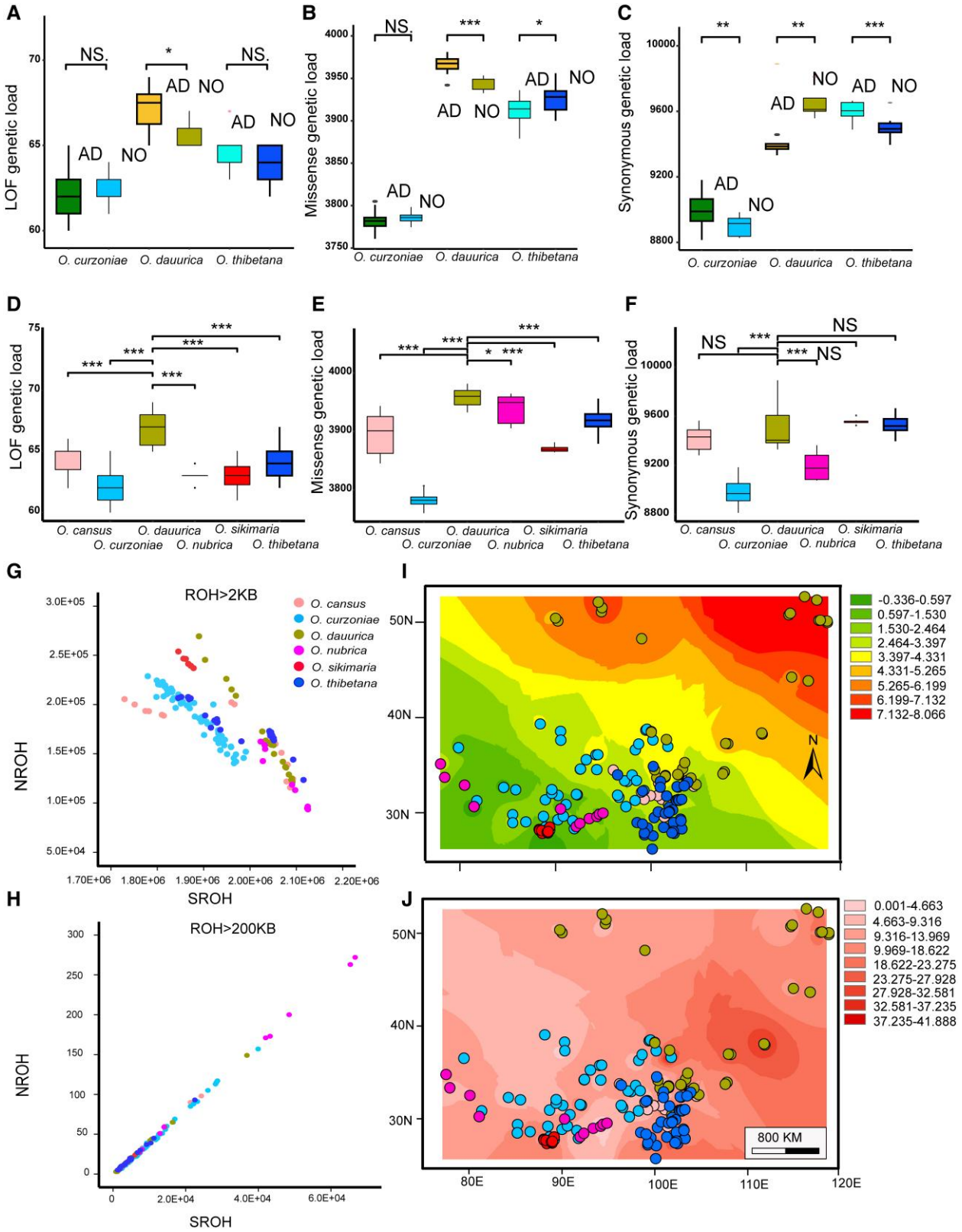

Fig. 6. Genome genetic loads and inbreeding depression tested by ROH and environmental changes in the sampling locations. (*A*–*C*) Comparing genome genetic loads in the admixed (AD) and nonadmixed (NO) populations. (*D*–*F*) Comparing genome genetic loads among species. (*G*, *H*) Comparing the sum total length of ROH (SROH) versus the total number of ROH (NROH) by >2 and 200 kb, respectively, among species. (*I*) Amplitude of temperature change within the range of sampling localities from LIG to LGM. Figure legends give the amplitude of temperature change between the LIG and LGM. (*J*) Human impacts within the range of sampling localities. The figure legend gives the human impact index from Theobald et al. 1990. The map shows the location of molecular voucher specimens of the six focal species in the QHTP and surrounding area (see fig. 1*B*).

history of introgression at the genome level in the context of environmental envelope modeling of historical distributions for a scenario that involved gene exchange at different periods of lineage evolution during the Pleistocene. In this framework, we then investigated the fate of introgressed genomic regions and their possible impact on the persistence of introgressed lineages. Contrary to other well-known cases demonstrating the elimination of small populations due to hybridization with large populations of expanding close relatives (Edmands 2007; Mobley et al. 2019), we find a complex history of multiple introgressions affecting nuclear and mitochondrial markers that suggest positive impacts on peripheral, partly inbred populations at the outer regions of the QHTP, consistent with the notion of genetic rescue.

In an era when multilocus sequencing is the main method in phylogenetic reconstruction, extensive introgression has been recognized from the incongruence of mitochondrial markers with the established morphological species boundaries (Shaw 2002; Joseph 2021), resulting in the widely held view that mitochondrial markers behave differently from nuclear loci; however, the data for assessing these loci have been limited. In *Ochotona*, mitochondrial markers were indeed an early indication of introgression and were used here as a convenient indicator of separating cohorts of presumed admixed and nonadmixed populations whereas also producing a time frame for four separate hypothesized introgression events that then indicated striking differences in the nuclear genomes that were apparently also affected by the same introgression events (in addition to other types of introgression that were also of great importance to lineage evolution; see below).

In this study, the ancestry admixture proportion tested by Admixture was consistent with the expectation from mitogenome introgression in *O. nubrica* and *O. curzoniae* but not in the other cases (fig. 4*B*). Genetic clustering algorithms, such as Admixture (Alexander et al. 2009) and STRUCTURE (Pritchard et al. 2000), have been widely used to detect population genetic structure (Lawson et al. 2018), with successful examples mainly from recent admixture between highly differentiated populations (Rosenberg et al. 2002; Bryc et al. 2010). However, minor parents' ancestry composition decreased dramatically after hybridization within several generations and left scattered short fragments in the recipient genome (Moran et al. 2021). These methods do not explicitly fit a historical model or unrealistically assume that all populations have radiated from a single ancestral group (Malinsky et al. 2018), thus these methods are not appropriate for studying ancient introgression, for example, they failed to identify introgression between *O. cansus* and *O. dauurica* in this study. Clustering methods were then replaced by the D-statistic (Durand et al. 2011) and its upgraded algorithms (Lambert et al. 2019; Malinsky et al. 2021), as well as many methods for inferring local ancestry, detecting the direction and strength of gene flow in both recent and ancient hybridization events (Kuhlwilm et al. 2016; Zheng and Janke 2018; Shirsekar et al. 2021; Pan et al. 2022). These methods provided the opportunity to explore unresolved questions about the genomic and evolutionary consequences of hybridization.

In addition, the direction and strength of gene flow identified by TreeMix, D-statistic, f_4-ratio, f-branch method, and GphoCS were slightly different. Malinsky et al. (2018) found TreeMix correctly inferred gene flow edges in the model with weak gene flow when the migration event was set to one, but it gave misleading results in more complex models. This was in agreement with our study of identifying misleading migration events when $m > 3$ (supplementary fig. S7, Supplementary Materials online). The slight inconsistency of D-statistics and f_4-ratio probably dues to their sensitivity to population size and the extinction of closely related sister specie in this subgenus. Zheng and Janke (2018) found D-statistic was robust against a wide range of genetic distances (divergence times), but it was sensitive to population size. Moreover, they also emphasized that D-statistics is qualitative and cannot be used to estimate the strength of gene flow (Zheng and Janke 2018). The sample size of six target species in this study ranged from 6 (*O. sikimaria*) to 67 (*O. curzoniae*), which likely influenced results in D-statistic and f_4-ratio tests. The results of the f-branch and GphoCS were more consistent, likely due to their methodological improvements. The former disentangled correlated f4-ratio results and aided in assigning the gene flow to particular branches on the population or species tree, the latter excluded highly variable genomic regions, and the influence of sample size was excluded. Notably, GphoCS needs high-performance computation resources, which limited us by using three individuals for each species in analyses. For hybridization events that occur across different timescales in many overlapping species ranges, it is still difficult to accurately locate and distinguish introgressed genomic components of diverse ancestry species, nor can we accurately date the time of these hybridization events, then methodological improvement in this field is needed to explore more deep level questions.

Adaptive Introgression in Pikas

Although the discovery of introgression was initially guided by mitochondrial markers, we identified genomic introgression between species that did not show a distinct signal of mitochondrial introgression based on the current dataset. For example, gene flow between *O. curzonae* and *O. thibetana*, between *O. curzoniae* and *O. dauurica*, and between *O. cansus* and *O. thibetana* was detected. Recurrence of adaptive genomic introgression was demonstrated by a large number of shared genes identified in both recent (from *O. nubrica* to *O. curzoniae*) and ancient (from *O. cansus* to *O. dauurica*) hybridization, which is potentially relevant to periodic environmental changes in the Quaternary. Hybridization introduces the introgression of alleles that aid species in coping with extreme environments and local adaptation (Legras et al. 2018; Hsieh et al. 2019). Compared with those of the nonadmixed

populations of *O. dauurica* in northeastern Asia, the elevational distributions of the admixed populations in the northeastern QHTP were significantly elevated.

Early hybridization has wider influences on the genome when compared with that of ancient hybridization, for example, we identified widespread genomic introgression during the early hybridization in *O. curzoniae*, but only a few genomic fragments were selectively fixed through the long evolution process, which was evidenced by a small proportion of fixed sites in the admixed *O. dauurica*. As ecologically advantageous traits are passed from donor to recipient, the selection from the environment will favor the maintenance of introgressed material (Liu et al. 2015). Here, alleles of key nuclear genes, such as *HTR7* and *ATP2A3*, related to intracellular calcium homeostasis, sensory properties, and response to ATP were identified as introgressed and fixed elements in *O. dauurica*. The intracellular balance of calcium and ATP plays an essential role in extremely cold environments (Brookes et al. 2004; Brinkkoetter et al. 2008) and is vital for high-altitude adaptation. The genes in the *FST* outlier region of admixed *O. dauurica* on chromosome 7A experienced extensive interspecific introgression. These genes are related to the balance of the intracellular physiological environment, development, and sperm capacitation. Here, two key genes, *SLC26A3* and *DLD*, hitchhiked on chromosome 7A, are both essential for sperm development and capacitation (Chávez et al. 2012; Panneerdoss et al. 2012; Khouri et al. 2018). During this process, reproductive isolation between different populations was enhanced, and then these adaptive introgressions likely play important role in early speciation in *O. dauurica*.

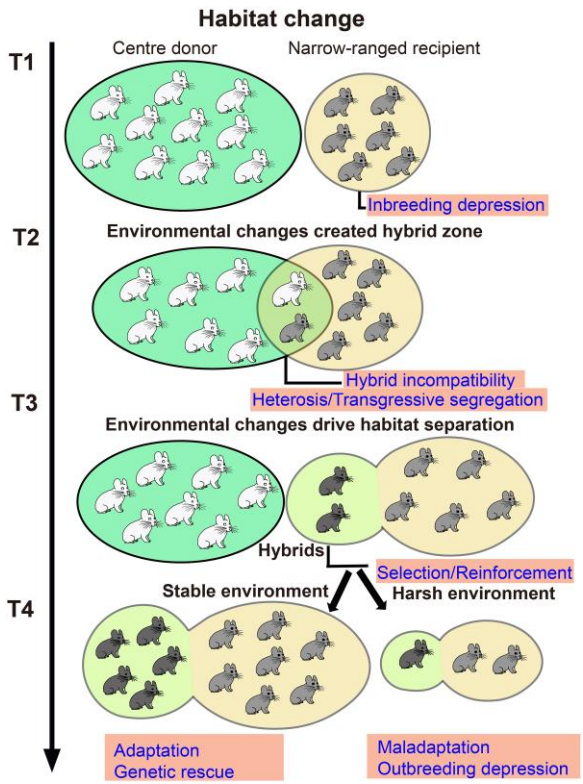

Fig. 7. A general model for the hybridization process in pikas. T1–T4 give different timescales in hybridization.

In short, we identified several coding regions within putative introgressed loci, likely contributing to the adaptation and differentiation of admixed *O. dauurica* on the highland in the northeast edge of the QHTP from its conspecific populations in its lowland northern species ranges (Mongolia and Russia). These genes are associated with local adaptation to a higher elevation. Generally, the dominant plateau pika is the primary source of gene flow to peripheral species; this indicates that global warming is driving the migration of climate-sensitive species to a higher altitude, the central plateau pika is expanding its species region, and genomic introgression from a higher altitude may play an essential role in the genetic rescue of lower altitude recipients. The recurrence of genomic introgression at different timescales implies convergences in genes under similar selection in nature. Adaptive introgression is a common aspect of species divergence and speciation, given the future fate of the recipient species, this mechanism is likely a type of evolutionary rescue that is from genetic variation obtained from hybridization.

Genomic Consequences and Demographic Response to Hybridization

The genomic consequences and demographic response of hybridization shown by pikas are much more complex than anticipated based on previous hypotheses and suggest that short-term changes in the genome are not sufficient to reflect the consequences of hybridization. Gene flow and environmental changes that occur at different times likely affect the evolutionary dynamics of peripheral species jointly. Genetic rescue is possible only if natural resources are abundant and the original constraints that induce population size decline are removed (Kottler et al. 2021). We postulate four stages of the hybridization process based on the observations made on pikas (fig. 7): 1) before hybridization, donor and recipient species diverged from each other mostly uniformly across all genomic regions (T1); 2) immediately after hybridization (facilitated by range shifts under environmental changes), the overall genetic diversity is elevated (T2); temporary heterosis, transgressive segregation, or hybrid incompatibility (including inbreeding depression) appear during this stage; 3) some introgressed elements may become fixed in recipient populations (T3), and this is possibly driven by selection or reinforcement to overcome hybrid incompatibility introduced by exogenous genes (Servedio and Noor 2003; Matute 2010; Kyogoku and Kokko 2020); and 4) the outcome of hybridization may depend on the amplitude of environmental change (T4). Genetic rescue and demographic recovery may predominate in stable environments, as exemplified by the ancient introgression from an extinct species to *O. thibetana*. However, the deterioration of the environment may lead to widespread maladaptation or outbreeding depression, leading to demographic decline, such as that presented in *O. dauurica*. This whole process

took at least 0.7 Mya in *O. dauurica* according to the comparison of the time when hybridization occurred and the demographic dynamics of the admixed lineage distinctly deviated from those of the nonadmixed lineage (supplementary fig. S18, Supplementary Material online).

Demographic Dynamics of Pikas and Conservation Implications

In addition, these events must be seen in the context of the partly known climatological history of the QHTP and surrounding areas in terms of the history of populations and their demographics as well as their potential for hybridization. Vegetation over the past 1.74 million years from the Zoige Basin on the QHTP showed three intervals of climatic oscillations (Zhao et al. 2020). Pikas are thermally sensitive with a highly fragmented patchy distribution, and these species responded to climate change with rapid demographic dynamics and range shifts in the late Quaternary (Galbreath et al. 2009). Interestingly, we identified three waves of demographic dynamics in *O. cansus*, *O. curzoniae*, *O. nubrica*, and *O. thibetana* in the last one million years with a dramatic population boom in the past two thousand years. These results again highlight pikas as sentinal species for detecting environmental changes and keystone species of the alpine ecosystem (Smith and Foggin 1999). This point of view was supported by a recent study that considered pikas as potential umbrella species that benefitted several co-occurring species (Sumbh and Hof 2022). Unlike the highly homogenous habitats in the central QHTP, an outstanding heterogeneous environment of surrounding mountains provides suitable microhabitats for different sublineages of peripheral pika species, which likely contributes to intraspecific differentiation and distinct demographical dynamics in response to climate change. Remarkably, the demographic dynamics of admixed populations in *O. thibetana* and *O. dauurica* prominently deviated from other lineages, which indicates that hybridization events influenced the evolutionary trajectories of recipients.

In a broad sense, a general trend of demographic decline of both center and peripheral pikas before six thousand years ago was correlated with global climate warming (Cooper et al. 2015; Wan and Zhang 2017), whereas subsequent population size increases in *O. curzoniae*, *O. cansus*, *O. nubrica*, and *O. thibetana* within 2000 to 600 years may have been linked to the massive extinction and range contraction of megafauna that occurred with the decrease in predation and competition (Malhi et al. 2016). Prior to that, climatic factors affected the distributions; in particular, *O. nubrica* suffered dramatic habitat fragmentation on the western edge of the QHTP during the LGM (fig. 3*E*), which then resulted in inbreeding depression (Ceballos et al. 2018). The dramatic demographic decline in *O. dauurica* continues to date in central and northern China and in Mongolia. The vegetation of this region is more sensitive to climate changes than that of the QHTP (Seddon et al. 2016), leading to a reduction in population size and consequently inbreeding (Bertorelle et al. 2022). *Ochotona sikimaria* inhabits a small region on the border between China and India, with distinct geographical boundaries restricting its range and demographic recovery. The demographic decline of this species coincided with the middle Holocene Climate Optimum (9000–5000 years) (Bova et al. 2021). Unlike the peripheral species, *O. curzoniae* obtains a small amount of genomic introgression from peripheral species and has the lowest genomic genetic loads and a lower level of inbreeding depression compared with other species. These genomic characteristics likely underlie its large population size and wide distribution, which offered opportunities to interact with different peripheral species during climatic oscillations.

The ecosystem of the QHTP and its vicinity is primarily regulated by climate with a lower level of human impact (Jacobson et al. 2019), which is beneficial to maintaining a home for cold-tolerant alpine species and the sustainability of high biodiversity. Apart from three hybrid zones for pikas, the QHTP and its vicinity were also reported to harbor hybridization of birds (Zhang, Tang, et al. 2019), lizards (Gao et al. 2022), and plants (Wu et al. 2022). The frequent occurrences of hybridization events in different taxa over time imply that the QHTP and its surrounding mountains are prime regions for gene flow in nature. This region is also a climate refugia for terrestrial and aquatic biota (Yang et al. 2009; Wen et al. 2016). From the perspective of genomic evolution, these hybrid zones are genetic refugia for species to acquire new genetic adaptations. The success of genetic rescue in nature or aided by humans largely depends on habitat size and quality (Ralls et al. 2020; Robinson et al. 2021). Therefore, conservation management should aim to improve habitat stability in hybrid zones to maintain the sustainability of these key evolutionary processes.

In summary, phylogenetic reconstruction and inferences of gene flow revealed at least four waves of mitochondrial introgression in the subgenus *Ochotona*, occurring at different times of lineage evolution and with distinct evolutionary outcomes. Introgression of the nuclear genome also occurred widely, in part associated with the same events, but only affecting a small proportion of the genomes and generally indicating a direction of gene flow from *O. curzoniae* distributed in the central plateau to species at the periphery. These genomic differences may be directly associated with adaptation to extreme environments on the QHTP and the early speciation in pikas, which is supported by the inferred localization of past hybrid zones surrounding the QHTP (supplementary fig. S3*D*, Supplementary Material online). Interspecific introgression followed presumed long-term endogamy and thus could have alleviated inbreeding depression (in *O. nubrica*). Ironically, even with hybridization-introduced genomic novelties, pikas in harsh environments (*O. dauurica* and *O. sikimaria*) suffered a dramatic demographic decline exacerbated by severe anthropogenic environmental changes affecting demographic recovery. These results emphasize that environmental stability and abundant food resources are key to the success of "genetic rescue" in nature and highlight the unique role of the QHTP and its vicinity in maintaining biodiversity.

Materials and Methods

Sampling

The specimens of pikas used in this study are preserved in the Institute of Zoology, Chinese Academy of Sciences (IOZCAS), and National Institute for Communicable Disease Control and Prevention, Chinese Centre for Disease Control and Prevention (CCDC), Zoological Museum of Moscow State University (ZMMU). These specimens were collected using line transect methods during the field survey of rodent-borne diseases and animal diversity between 2001 and 2021. In total, 403 new specimens were collected in this study. Specimens were dissected immediately with muscle or liver samples preserved in 95% ethanol. These samples were transferred to a −80 °C freezer before being sent for sequencing. Detailed information for these specimens is provided in supplementary table S4, Supplementary Material online.

Morphological Study

We digitized the cranium shapes of *O. cansus*, *O. curzoniae*, *O. dauurica*, *O. nubrica*, *O. sikimaria*, *O. thibetana*, and *O. thomasi* based on 17 landmarks in the dorsal view and 23 landmarks in the ventral view using tpsDig version 2.3v (Rohlf 2005). The locations of the landmarks are given in supplementary figure S1, Supplementary Material online. The coordinates of each landmark were aligned, and the effects of their location, orientation, and scale were removed through a generalized Procrustes analysis using the geomorph R package (Adams and Otarola-Castillo 2013). We conducted a principal component analysis to explore the breadth of cranial morphospace variation within the subgenus *Ochotona* and used ANOVA to test for significant morphological differences. All analyses were performed using the geomorph package. Collection information of specimens included in the analyses is provided in supplementary table S1, Supplementary Material online.

Sequencing of *CYTB*

We sequenced *Ochotona* specimens ($n = 328$) collected by IOZCAS, CCDC, and ZMMU. Total genomic DNA was isolated from muscle using the Qiagen DNeasy Blood and Tissue Kit (Qiagen China, Pudong, Shanghai, China). The primer sequences used for PCR and sequencing and their original reference were from Galbreath et al. (2009). All PCR products were sequenced with an ABi 3730 automatic sequencer (Perkin-Elmer, Waltham, MA). Accessions of new *CYTB* sequences are given in supplementary table S4, Supplementary Material online.

Sampling, Sequencing, and Filtering the Genome Data

One hundred fifteen newly collected samples assigned to the subgenus *Ochotona* based on their morphological identifications and phylogenetic analyses of *CYTB* were selected for whole-genome sequencing. These samples included *O. cansus* ($n = 15$), *O. curzoniae* ($n = 67$), *O. dauurica* ($n = 17$), *O. nubrica* ($n = 10$), and *O. sikimaria* ($n = 6$). Moreover, one sample of *O. argentata* and 27 individuals of *O. thibetana* were available from a previous study (Ge et al. 2022). A total of 1.5 μg of DNA per sample was used as the input for DNA library preparation. Whole-genome DNA was fragmented to an average size of 350 bp by Covaris S220. Sequencing libraries were generated using a TruSeq Nano DNA HT sample preparation kit (Illumina USA). Index codes were added to trace the sequences of each sample. DNA fragments were end polished, A-tailed, and ligated with a full-length adapter for sequencing. Finally, the PCR products were purified (AMPure XP system), and these libraries were analyzed to determine their size distribution on an Agilent 2100 Bioanalyzer and then quantified using real-time PCR. The libraries constructed as described above were sequenced on the Illumina NovaSeq platform (2×150 bp paired-end). Sequencing was performed by Berry Genomics (Beijing, China). The raw read data of each sample were tested and filtered using fastp (Chen et al. 2018). Low-quality bases with Phred scores <30 were clipped from the 5′ and 3′ ends of the reads. Adapters and low-quality and duplicated reads were filtered out. The quality of the cleaned data was tested using FASTQC (Schmieder and Edwards 2011). Collection information and data size of each sample are given in supplementary table S5, Supplementary Material online. Sequencing was conducted by Berry Genomics (Beijing, China). Original data were submitted to the China National GeneBank DataBase (CNP0002399).

Reference-Based Assembly

We mapped the clean reads of all sequenced individuals by using the genome of *O. princeps* (Sjodin et al. 2021, GCF_014633375.1_OchPri4.0) as a reference in BWA (Li and Durbin 2009). The source files generated in this step were then sorted and filtered by removing PCR duplicates, indels and low-quality sites in SAMtools (Li et al. 2009). After filtering, an average of 107,758,998 single nucleotide polymorphisms (SNPs) were retained for each individual (supplementary table S5, Supplementary Material online). A total of 143 vcf files of the subgenus *Ochotona* together with one individual of *O. argentata* were merged into one vcf file for the following analyses (bcftools merge -m snps -f PASS, –force-samples) (Danecek et al. 2011). This dataset was filtered to remove indels and sites with any missing genotypes, and only biallelic sites were kept in the following analyses. The final dataset included a total of 14,959,431 SNP sites.

Phylogenetic Reconstruction

We established four datasets to reconstruct the phylogeny of sequenced individuals: 1) the *CYTB* newly generated in the present study and those available from GenBank; 2) the MTGs of 115 individuals who were freshly sequenced in the present study plus those of *O. thibetana* available from a previous study (Ge et al. 2022) and *O. princeps*

(NC005358) from GenBank; 3) the SCOs extracted from the contig files of the whole-genome sequencing data of the same specimens; and 4) the MTGs generated in the present study and those available from GenBank. Complete MTG sequences and whole genomes of *O. princeps* (AJ537415), *Lepus timidus* (KR019013), *Oryctolagus cuniculus* (AJ001588), and *Lepus americanus* (KJ397613) were downloaded from GenBank. These taxa were used as outgroups in the phylogenetic reconstruction.

CYTB was aligned in Muscle (Edgar 2004) and partitioned by codon position. The best nucleotide substitution model for each partition was chosen in PartitionFinder 3.8.31 (Lanfear et al. 2017). Bayesian analyses were conducted in Mrbayes 3.2 (Ronquist et al. 2012) with four chains, each chain consisting of 80 million generations with the first 25% discarded as burn-in, and the final tree was visualized in Figtree v. 1.4.0 (Rambaut 2010). Moreover, we ran a maximum likelihood analysis using IQ-Tree (Nguyen et al. 2015). Detailed information for *CYTB* sequences included in these analyses is provided in supplementary table S4, Supplementary Material online.

The MTGs and autosomes were assembled by different pipelines using clean reads. First, we used GetOrganelle (Jin et al. 2020) to assemble the MTGs from the whole clean data. MTGs from GenBank and those newly generated in the present study were annotated by the online server MITOS (Bernt et al. 2013). Thirteen protein-coding sequences extracted from MTGs were aligned using MUSCLE and concatenated together. We used PartitionFinder 3.8.31 to select the most appropriate partition sets for this dataset. We performed Bayesian inferences using MrBayes 3.1.12. We also conducted a maximum likelihood analysis using IQ-Tree. Whole mitochondrial DNA sequences with annotation information from newly sequenced samples were submitted to GenBank under accession numbers OP005990–OP006107, and detailed information for these data is provided in supplementary table S6, Supplementary Material online.

The de novo assembly of nuclear orthologs from each sequenced individual was conducted using MEGAHIT 1.2.9 (Li et al. 2015). During this analysis, clean reads were assembled into contig files that were used to extract SCOs in the following analyses. Moreover, we used BUSCO 3.0.2 (Simão et al. 2015) to estimate the percentage of expected conserved SCOs captured in our assemblies using the database of glires as a reference, which was provided by OrthoDB 10 (Zdobnov et al. 2020). BUSCO is software for assessing genome assembly and annotation completeness with SCOs. OrthoDB is a leading resource of evolutionary and functional annotations of orthologs.

To extract SCOs from the whole-genome data, we used the final contigs resulting from the MEGAHIT assembly as input data. We aligned the protein sequence from each of the reference species of glires to that from newly assembled individuals using TBLASTN (Boratyn et al. 2013). All coding domains in the assemblies were predicted by metaeuk (Karin et al. 2020). The protein sequences of SCOs were extracted and aligned in MAFFT (Nakamura et al. 2018), and we used Gblocks 0.91b (Talavera and Castresana 2007) to remove the highly variable regions in the alignments of each ortholog. We inferred the gene trees of 6710 SCOs in FastTree (Price et al. 2010). Each SCO has at least four individuals present in the dataset. The gene trees were used to infer the species tree in ASTRAL-III (Zhang et al. 2018).

Identification of Overall Gene Flow Among Species at the Genomic Level

To test the gene of flow among genetic lineages, we used four different software programs. We first used ADMIXTURE (Alexander et al. 2009), a software tool for maximum likelihood estimation of individual ancestries from multilocus SNP genotype datasets. In these analyses, the outgroup species were removed from the dataset, and the genotypes were subset to the respective candidate regions and converted to plink format (Purcell et al. 2007). Admixture was run with *k* values between 6 and 9 for each region. In the second procedure, we pruned the original file of the vcf file in high LD. Sites with missing values were removed from the analyses. The filtered vcf file and a file that provided the information on species assignment were used as inputs. Migration edges (0–5) were set with *O. argentata* being used as an outgroup. plotting_funcs. R was used to plot the results. These analyses were conducted in Treemix (Pickrell and Pritchard 2012). The optimal number of migration edges was determined by OptM (Fitak 2021). Then, we used Dsuite (Malinsky et al. 2021) to calculate the strength of gene flow among the six species by three different methods: the D-statistics (Durand et al. 2011), f4-ratio (Patterson et al. 2012) and "f-branch" method (Malinsky et al. 2018). A phylogenetic tree that included one individual from each of the six genetic lineages generated in the above analyses was used in the analyses, and each individual was assigned to corresponding species in a sample set file. *O. argentata* was used as an outgroup. First, we run "Dsuite Dtrios' by using the merged vcf file, the tree file, and the sample sets file as input. In these analyses, we obtained the overall statistics among species. Second, we run "Dsuite Dinvestigate -w 50,25" by using the vcf file, the sample sets file, and the trio-set file as input. In this analysis, we identified the strength of gene flow in different regions along individual chromosomes. The "-w 50,25" option specified that the statistics should be averaged over windows of 50 informative SNPs, moving forwards by 25 SNPs at each step. Third, we conducted "Dsuite Fbranch" by using the phylogenetic tree and the result obtained from the "Dsuite Dtrios" analysis as input, which helped in mapping the strength of gene flow with the topological structure of the tree. These results were visualized in "plot_d.rb," "plot_f4ratio.rb" of Dsuite, and "ggplot2" of R packages (Wickham 2016).

Moreover, we used G-PhoCS (Gronau et al. 2011) to identify the time, direction, and strength of gene flow among species. We excluded genomic regions that were likely to have evolved under the effect of strong natural

selection, including exons of protein-coding genes and the 2 kb flanking them on each side, as well as repeat elements and conserved noncoding elements. Moreover, sites with missing data were also removed. After filtering, 16,517,000 sites remained in the following analyses. We extracted 1 kb loci from these sites. We ran MCMC analyses using 1,000 loci by setting up migration bands between species and ancestor branches. The MCMC chain was run for 80 million generations and sampled every 20 generations. We set up 31 migration bands that included each pair of these species as source and target species.

Identification of the Introgressed Segments in the Admixed Populations

Six individuals of *O. curzoniae*, one individual of *O. nubrica*, 11 individuals of *O. dauurica*, and three individuals of *O. thibetana* appeared as MTG-admixed individuals. These results indicated that at least four waves of mitochondrial introgression occurred in the subgenus *Ochotona*, which offered the opportunity to uncover the genomic consequences of genomic introgression across different time scales. To identify nuclear genes potentially associated with introgression at different timescales, we set the admixed populations of *O. curzoniae* and *O. dauurica* as target datasets.

The identification of the admixture populations was based on three methods. First, we considered the results of Admixture. Second, we used Twisst (topology weighting by iterative sampling of subtrees, Martin and Belleghem 2017), a simple, descriptive method designed for exploring how relationships vary across the genome using population genomic data due to both variations in lineage sorting and introgression. Moreover, we defined the populations ($n > 3$) of *O. curzoniae* and *O. dauurica* based on their geographical localities and then used Dsuite (Malinsky et al. 2021) to determine which populations have significant gene flow with minor parent species (here, our focus species pairs were *O. curzoniae* and *O. nubrica* and *O. dauurica* and *O. canus*).

We identified the local ancestry of each segment in the genome of admixed populations using Loter (Dias-Alves et al. 2018). This fast and parameter-free software makes genomic studies about admixture processes more accessible. We annotated the genes present in the admixed populations (from CN and PL) of *O. curzoniae* and *O. dauurica*. Local ancestry inference in Loter was conducted by removing all sites with missing data. The filtered vcf files were split into 33 files according to the chromosome number of the reference genome. Then, we ran Loter using the admixed populations of *O. curzoniae* as the recipient population, and the nonadmixed *O. curzoniae* and *O. nubrica* were used as the donor populations. Similarly, the admixed populations *O. dauurica* identified in the above analyses were used as recipient populations, and the nonadmixed *O. dauurica* and *O. cansus* were used as donor populations. During these analyses, sites considered as introgressed were marked as "1," whereas those not suffering introgression were marked as "0". Sites marked as "1" in all individuals were considered "fixed". As the donor for the admixed populations of *O. thibetana* was extinct, that species could not be used for local ancestry inference in Loter. To evaluate the ancestry of fixed SNP sites in *O. dauurica*, we extracted these sites from the whole dataset and defined them as a file that included fixed sites from introgression for *O. dauurica*. We calculated the pairwise distance between individuals in vcf2dis (https://github.com/BGI–shenzhen/VCF2Dis) and inferred the phylogenetic relationship between individuals using FastMe2.0 (Lefort et al. 2015). Annotation of identified loci or genomic regions was conducted in snpEff (Cingolani et al. 2012) using the genome of *O. princeps* as a reference. Enrichment of biological processes was conducted in Shinygo (Ge et al. 2020) by using the American pika and the mouse as background species because the reference genome of the American pika remains poorly annotated with a large number of genes with undetermined GeneID. The top twenty biological pathways with significant FDR values ($P < 0.05$) were retained for further analyses.

Identifying "Genomic Island of Differentiation"

To identify genomic region of differentiation between admixed and noadmixed populations, as well as between these populations with the donor species, we calculated F_{ST} and *Dxy* by setting 1) the admixed *O. curzoniae*, nonadmixed *O. curzoniae*, and *O. nubrica* as separate target groups and 2) the admixed *O. dauurica*, nonadmixed *O. dauurica*, and *O. cansus* as separate target groups. A sliding window of 50 kb with a step size of 10 kb was used in these analyses. These analyses were conducted in VCFtools (Danecek et al. 2011) and scripts in genomics_general (https://github.com/simonhmartin/genomics_general) using the aforementioned filtered vcf files.

To further evaluate whether there is enhanced genomic differentiation between recipient and donor in the target genomic region, we also followed Scherz et al (2022) to test the heterogeneity in local topological weightings using genomic sliding window trees. A window size of 250 SNPs and the GTRGAMMA model in RAxML (Stamatakis 2014) was implemented to reconstruct local trees along the chromosome. Trees were summarized in TWISST by defining admixded and nonadmixed *O. dauurica* as separate groups. Heterogeneity in local topological weightings along the chromosome was visualized in ggplot2.

Inferring the Demographic History

We used three different methods to infer the historical and recent demographic history of six species in *Ochotona*. First, we used the PSMC model (Li and Durbin 2011) to examine demographic history based on individual contig files of the genomic data for each genetic lineage identified in the above analyses. We used the contig files that were obtained in the above assemblies from MEGAHIT to regenerate 20 pseudochromosomes for each individual. Then, the contig files of each individual were randomly merged to regenerate 20 pseudochromosomes using Fatools in iTools (He et al. 2013). We mapped the clean

reads back to the newly generated pseudochromosomes individually. Next, we used BWA (Li and Durbin 2009) and SAMtools (Li et al. 2009) to convert the aligned results to bam files. We sorted the bam files and built an index for the sorted file. We estimated genotype likelihoods with an adjusted mapping quality greater than 50. We used BCFtools (Li 2011) to identify SNPs. We used the file generated in the above step to conduct PSMC analysis. We converted the format of consensus sequences using fq2psmcfa. After transformation, the population history of each species was inferred by PSMC. The historical literature indicated that pikas need approximately half a year to reach sexual maturity (Lissovsky 2016); we used 0.5 years as the generation time and 2.96×10^{-9} as the mean mutation rate for nuclear protein-coding genes as pikas are similar to wild rats in size (Teng et al. 2017; Zeng et al. 2018). In the second method, we used SMC++, which can jointly infer population size histories and split times in diverged populations. It employs a novel spline regularization scheme that significantly reduces estimation error (Terhorst et al. 2017). VCF files generated by mapping clean reads to the reference genome, *O. princeps*, were used as input data. Moreover, during the inference of gene flow in G-Phocs (Gronau et al. 2011) using the neutral loci, we also analyzed the demographical size at the same time. It was calculated using the θ value, calculated by $\theta=4N_e\mu$, in which N_e is the total effective population size and μ is the average mutation rate; we assumed $\mu=2.96 \times 10^{-9}$.

Testing Genome Genetic Loads and Inbreeding Depression

Inbreeding depression is one of the major outcomes of intraspecific hybridization. Here, we measured genome-wide ROH, the indicator of genomic autozygosity, to compare the evolutionary history among species (Ceballos et al. 2018). This analysis was conducted in Plink (Purcell et al. 2007) using filtered VCF files of sequence individuals as input. The difference in total length of ROH identified by limiting the length to 2 and 200 kb for each species was compared. Rapid climatic changes and increases in human impact are usually considered external factors that drive demographic decline in nature. Moreover, an increase in outbreeding and genetic loads is the primary genomic reason that leads to rapid demographic decline (Hu et al. 2020; Wang, Burley, et al. 2020; Bertorelle et al. 2022). We compared the overall genome genetic loads among six species by annotating the biallelic SNP sites presented in all individuals. We annotated all SNP sites by excluding sites with missing information that avoided the influence of sequencing depth and coverage in different samples. *O. argentata* was used as an outgroup taxon. We categorized genome genetic loads into three types: variants that cause loss of function (LOF genetic load), missense genetic load, and synonymous genetic load. We annotated all of these sites in snpEff using the genome of *O. princeps* as a reference. We ran ANOVAs on the values of these types of genetic loads among species and between admixed and nonadmixed populations to test the significance of their difference.

Ecological Niche Modeling

We assessed range shifts of the five target species over time by building LIG and LGM, future (MIROC-ESM, rcp45, 2070), and present ENMs. Bioclimatic variables of WorldClim and elevational grids of 2.5 min spatial resolution were used as ecological predictors (Fick and Hijmans 2017; Karger et al. 2017). Species occurrence was mainly based on collecting information from the molecular voucher specimens. To reduce spatial autocorrelation and sampling bias, we excluded duplicated localities within a 50 km resolution grid and controlled Moran's I after each modeling run. If Moran's I was above 0.2, we rarified points by distance, sequentially increasing the distance value, starting from 10 km. The test sample was obtained by rarifying the initial dataset using a similar procedure, but the grid resolution and rarifying distance were 1.1-fold larger.

We used the "maxent.jar" algorithm implemented in ENMeval 2.0.3 R package (Muscarella et al. 2014; Kass et al. 2021) to build Maxent models with a set of parameters, using regularization multipliers ranging from 0.75 to 3 with four combinations of feature classes (L, LQ, LQH, and LQHP, where L = linear, Q = quadratic, *P* = product, and H = hinge). We calculated the principal component set based on predictors, and for each species, we selected only the PCs whose permutation importance was above 2% in the preliminary runs. Selection of the best model was performed based on AICc, calculated on the test sample. Ten thousand background points were randomly selected for model calculation from the territory of the QHTP with a slightly (three times) higher probability of point selection within a 100 km buffer area around pikas occurrence points and a ten times higher probability of selection around grid cells of all pika species occurrence points.

Supplementary Material

Supplementary data are available at *Molecular Biology and Evolution* online.

Acknowledgments

We appreciate the valuable suggestions on the data analyses from Drs Ghislain Durif, Enrique Santiago Rubio, Ilan Gronau, Simon Martin, Shengkai Pan, Dexing Zhang, Yan Hao, Hua Chen, and Qiang Gao. We appreciate Prof Xin Zhou for providing the profile of *O. cansus*. We also appreciate great encouragement and help from Profs Zuojian Feng, Fuwen Wei, Xiangjiang Zhan, Yong Zhang, Weiwei Zhai, Chaodong Zhu, and Jiatang Li. We thank anonymous editors and reviewers for their constructive comments to improve this manuscript. This work was sponsored by the Second Tibetan Plateau Scientific Expedition and Research Program (No. 2019QZKK0402,2019QZKK0501)

and the National Nature Science Fund of China (31872958, 32170426 to D.Y.G. and 32271736 and 32170420 to W.Z.). D.Y.G. and A.P.V. were supported by a Newton Advanced Fellowship of the Royal Society, United Kingdom (NA150142). A.F. was financially supported by the Chinese Academy of Sciences President's International Fellowship Initiative (2021PB0021). A.L. worked under the research project of the Severtsov Institute of Ecology and Evolution, Russian Academy of Sciences, project no. AAAA-A18-118042490058-8.

Author Contributions

D.Y.G., Q.S.Y., A.P.V., and Y.H.Q. designed the research. D.Y.G., Z.X.W., L.L., A.L., A.F., J.L.C., D.P.M., X.L., and Q.S.Y. participated in sample collection. D.Y.G., A.F., A.L., D.Z.Z., H.S.S., Y.L.C., Y.C.C., W.Z., X.L.W., and Y.B.Z. performed the data collection and analyses. D.Y.G., Z.X.W., Y.H.Q., A.F., A.L., W.Z., A.P.V., and D.Z.Z. wrote the paper.

Data Availability

The datasets containing the accession numbers for *Ochotona* generated in this study are available as supplemental information. Original sequence reads of genome data are available at the China National Gene Bank (Accession number CNP0003365), and the assembled sequence of mitochondrial data are available at the National Center for Biotechnology Information Search database (Accession number OP005990–OP006107 and OP004351–OP004678).

References

Adams D, Otarola-Castillo E. 2013. Geomorph: an R package for the collection and analysis of geometric morphometric shape data. *Methods Ecol Evol*. **4**:393–399.

Alexander DH, Lange K. 2011. Enhancements to the ADMIXTURE algorithm for individual ancestry estimation. *BMC Bioinform*. **12**: 246.

Alexander DH, Novembre J, Lange K. 2009. Fast model-based estimation of ancestry in unrelated individuals. *Genome Res*. **19**(9): 1655–1664.

Arregoitia LDV, Leach K, Reid N, Fisher DO. 2015. Diversity, extinction, and threat status in Lagomorphs. *Ecography*. **38**(11): 1155–1165.

astillo Vardaro JA, Epps CW, Frable BW, Ray C. 2018. Identification of a contact zone and hybridization for two subspecies of the American pika (*Ochotona princeps*) within a single protected area. *PLoS ONE*. **13**(7):e0199032.

Bell DA, Robinson ZL, Funk WC, Fitzpatrick SW, Allendorf FW, Tallmon DA, Whiteley AR. 2019. The exciting potential and remaining uncertainties of genetic rescue. *Trends Ecol Evol*. **34**(12):1070–1079.

Bernt M, Donath A, Juhling F, Externbrink F, Florentz C, Fritzsch G, Putz J, Middendorf M, Stadler PF. 2013. MITOS: improved de novo metazoan mitochondrial genome annotation. *Mol Phylogenet Evol*. **69**(2):313–319.

Bertorelle G, Raffini F, Bosse M, Bortoluzzi C, Iannucci A, Trucchi E, Morales HE, van Oosterhout C. 2022. Genetic load: genomic estimates and applications in non-model animals. *Nat Rev Gen* **23**:492–503.

Boratyn GM, Camacho C, Cooper PS, Coulouris G, Fong A, Ma N, Madden TL, Matten WT, McGinnis SD, Merezhuk Y, *et al.* 2013. BLAST: a more efficient report with usability improvements. *Nucleic Acids Res*. **41**(W1):W29–W33.

Bova S, Rosenthal Y, Liu Z, Godad SP, Yan M. 2021. Seasonal origin of the thermal maxima at the Holocene and the last interglacial. *Nature*. **589**(7843):548–553.

Brinkkoetter PT, Song H, Losel R, Schnetzke U, Gottmann U, Feng Y, Hanusch C, Beck GC, Schnuelle P, Wehling M, *et al.* 2008. Hypothermic injury: the mitochondrial calcium, ATP and ROS love-hate triangle out of balance. *Cell Physiol Biochem*. **22**(1–4): 195–204.

Brookes PS, Yoon Y, Robotham JL, Anders MW, Sheu SS. 2004. Calcium, ATP, and ROS: a mitochondrial love–hate triangle. *Am J Physiol Cell Physiol*. **287**(4):C817–C833.

Bryc K, Velez C, Karafet T, Moreno-Estrada A, Reynolds A, Auton A, Hammer M, Bustamante Carlos D, Ostrer H. 2010. Genome-wide patterns of population structure and admixture among Hispanic/Latino populations. *Proc Natl Acad Sci U S A*. **107-**(Suppl_2):8954–8961.

Ceballos FC, Joshi PK, Clark DW, Ramsay M, Wilson JF. 2018. Runs of homozygosity: windows into population history and trait architecture. *Nat Rev Gen*. **19**(4):220–234.

Cevik V, Boutrot F, Apel W, Robert-Seilaniantz A, Furzer OJ, Redkar A, Castel B, Kover PX, Prince DC, Holub EB, *et al.* 2019. Transgressive segregation reveals mechanisms of *Arabidopsis* immunity to Brassica-infecting races of white rust (*Albugo candida*). *Proc Natl Acad Sci U S A*. **116**(7):2767–2773.

Chávez JC, Hernández-González EO, Wertheimer E, Visconti PE, Darszon A, Treviño CL. 2012. Participation of the Cl^-/HCO_3^- exchangers SLC26A3 and SLC26A6, the Cl^- channel CFTR, and the regulatory factor SLC9A3R1 in mouse sperm capacitation1. *Biol Rep*. **86**(1):1–14.

Chen SF, Zhou YQ, Chen YR, Gu J. 2018. Fastp: an ultra-fast all-in-one FASTQ preprocessor. *Bioinformatics*. **34**(17):884–890.

Cingolani P, Platts A, Wang le L, Coon M, Nguyen T, Wang L, Land SJ, Lu X, Ruden DM. 2012. A program for annotating and predicting the effects of single nucleotide polymorphisms, SnpEff: SNPs in the genome of *Drosophila melanogaster* strain w1118 iso-2 iso-3. *Fly (Austin)*. **6**(2):80–92.

Cooper A, Turney C, Hughen KA, Brook BW, McDonald HG, Bradshaw CJ. 2015. Abrupt warming events drove Late Pleistocene Holarctic megafaunal turnover. *Science*. **349**(6248): 602–606.

Danecek P, Auton A, Abecasis G, Albers CA, Banks E, DePristo MA, Handsaker RE, Lunter G, Marth GT, Sherry ST, *et al.* 2011. The variant call format and VCFtools. *Bioinformatics*. **27**(15): 2156–2158.

Delibes-Mateos M, Smith AT, Slobodchikoff CN, Swenson JE. 2011. The paradox of keystone species persecuted as pests: a call for the conservation of abundant small mammals in their native range. *Biol Conserv*. **144**(5):1335–1346.

Dias-Alves T, Mairal J, Blum MGB. 2018. Loter: a software package to infer local ancestry for a wide range of species. *Mol Biol Evol*. **35**(9):2318–2326.

Dirzo R, Young HS, Galetti M, Ceballos G, Isaac NJB, Collen B. 2014. Defaunation in the Anthropocene. *Science*. **345**(6195):401–406.

Durand EY, Patterson N, Reich D, Slatkin M. 2011. Testing for ancient admixture between closely related populations. *Mol Biol Evol*. **28**(8):2239–2252.

Duranton M, Allal F, Vali? re S, Bouchez O, Bonhomme F, Gagnaire PA. 2020. The contribution of ancient admixture to reproductive isolation between European sea bass lineages. *Ecol Lett*. **4**(3): 226–242.

Edgar RC. 2004. MUSCLE: multiple sequence alignment with high accuracy and high throughput. *Nucleic Acids Res*. **32**(5):1792–1797.

Edmands S. 2007. Between a rock and a hard place: evaluating the relative risks of inbreeding and outbreeding for conservation and management. *Mol Ecol*. **16**(3):463–475.

Feng SH, Fang Q, Barnett R, Li C, Han S, Kuhlwilm M, Zhou L, Pan HL, Deng Y, Chen GJ, *et al.* 2019. The genomic footprints of the fall and recovery of the crested ibis. *Curr Biol*. **29**(2):340–349 e347.

Fenster CB, Galloway LF. 2000. Inbreeding and outbreeding depression in natural populations of *Chamaecrista fasciculata* (Fabaceae). *Conserv Biol*. **14**(5):1406–1412.

Fick SE, Hijmans RJ. 2017. Worldclim 2: new 1-km spatial resolution climate surfaces for global land areas. *Int J Climatol*. **37**(12): 4302–4315.

Fitak RR. 2021. Optm: estimating the optimal number of migration edges on population trees using treemix. *Biol Methods Protoc*. **6**(1):bpab017.

Fitzpatrick SW, Gerberich JC, Angeloni LM, Bailey LL, Broder ED, Torres-Dowdall J, Handelsman CA, López-Sepulcre A, Reznick DN, Ghalambor CK, *et al.* 2016. Gene flow from an adaptively divergent source causes rescue through genetic and demographic factors in two wild populations of *Trinidadian guppies*. *Evol Appl*. **9**(7):879–891.

Frankham R. 2015. Genetic rescue of small inbred populations: meta-analysis reveals large and consistent benefits of gene flow. *Mol Ecol*. **24**(11):2610–2618.

Galbreath KE, Hafner DJ, Zamudio KR. 2009. When cold is better: climate-driven elevation shifts yield complex patterns of diversification and demography in an alpine specialist (American pika, *Ochotona princeps*). *Evolution*. **63**(11):2848–2863.

Gao W, Yu CX, Zhou WW, Zhang BL, Chambers EA, Dahn HA, Jin JQ, Murphy RW, Zhang YP, Che J. 2022. Species persistence with hybridization in toad-headed lizards driven by divergent selection and low recombination. *Mol Biol Evol*. **39**(4):msac064.

Ge DY, Feijó A, Wen ZX, Lissovsky A, Zhang DZ, Cheng JL, Yan CC, Mu DP, Wu XL, Xia L, *et al.* 2022. Ancient introgression underlying the unusual mito-nuclear discordance and coat phenotypic variation in the Moupin pika. *Divers Distrib*. **28**(12):2593–2609.

Ge SX, Jung D, Yao R. 2020. ShinyGO: a graphical gene-set enrichment tool for animals and plants. *Bioinformatics*. **36**(8):2628–2629.

Ge DY, Wen ZX, Xia L, Zhang ZQ, Erbajeva M, Huang CM, Yang QS. 2013. Evolutionary history of lagomorphs in response to global environmental change. *PLoS One*. **8**(4):e59668.

Ge DY, Zhang ZQ, Xia L, Zhang Q, Ma Y, Yang QS. 2012. Did the expansion of C_4 plants drive extinction and massive range contraction of micromammals? Inferences from food preference and historical biogeography of pikas. *Palaeogeogr Palaeoclimatol Palaeoecol*. **326–328**:160–171.

Goulet BE, Roda F, Hopkins R. 2017. Hybridization in plants: old ideas, new techniques. *Plant Physiol*. **173**(1):65–78.

Grant PR, Grant BR. 2019. Hybridization increases population variation during adaptive radiation. *Proc Natl Acad Sci U S A*. **116**(46):23216–23224.

Grayson DK. 2005. A brief history of Great Basin pikas. *J Biogeog*. **32**(12):2103–2111.

Gronau I, Hubisz MJ, Gulko B, Danko CG, Siepel A. 2011. Bayesian Inference of ancient human demography from individual genome sequences. *Nat Gen*. **43**(10):1031–1034.

He W, Zhao S, Liu X, Dong S, Lv J, Liu D, Wang J, Meng Z. 2013. Reseqtools: an integrated toolkit for large-scale next-generation sequencing based resequencing analysis. *Genet Mol Res*. **12**(4): 6275–6283.

Hsieh P, Vollger MR, Dang V, Porubsky D, Baker C, Cantsilieris S, Hoekzema K, Lewis AP, Munson KM, Sorensen M, *et al.* 2019. Adaptive archaic introgression of copy number variants and the discovery of previously unknown human genes. *Science*. **366-**(6463):eaax2083.

Hu J, Hao Z, Frantz L, Wu SF, Chen W, Jiang Y, Wu H, Kuang WM, Li HP, Zhang YP, *et al.* 2020. Genomic consequences of population decline in critically endangered pangolins and their demographic histories. *Natl Sci Rev*. **7**(4):798–814.

Jacobson AP, Riggio J, Tait A M, Baillie J EM. 2019. Global areas of low human impact ('low impact areas') and fragmentation of the natural world. *Sci Rep*. **9**(1):14179.

Jin JJ, Yu WB, Yang JB, Song Y, dePamphilis CW, Yi TS, Li DZ. 2020. Getorganelle: a fast and versatile toolkit for accurate de novo assembly of organelle genomes. *Genome Biol*. **21**(1):241.

Johnson H, Mills LS, Wehausen J, Stephenson TR, Luikart G. 2011. Translating effects of inbreeding depression on component vital rates to overall population growth in endangered bighorn sheep. *Conserv Biol*. **25**(6):1240–1249.

Joseph L. 2021. Mitonuclear ecology. *J Field Ornithol*. **92**(3):309–313.

Karger DN, Conrad O, Böhner J, Kawohl T, Kreft H, Soria-Auza RW, Zimmermann NE, Linder HP, Kessler M. 2017. Climatologies at high resolution for the earth's land surface areas. *Sci Data*. **4**(1):170122.

Karin E L, Mirdita M, Söding J. 2020. Metaeuk—sensitive, high-throughput gene discovery, and annotation for large-scale eukaryotic metagenomics. *Microbiome*. **8**(1):48.

Kass JM, Muscarella R, Galante PJ, Bohl CL, Pinilla-Buitrago GE, Boria RA, Soley-Guardia M, Anderson RP. 2021. ENMeval 2.0: redesigned for customizable and reproducible modeling of species' niches and distributions. *Methods Ecol Evol*. **12**(9):1602–1608.

Khouri E E, Whitfield M, Stouvenel L, Kini A, Riederer B, Lores P, Roemermann D, di Stefano G, Drevet JR, Saez F, *et al.* 2018. *SLC26A3* deficiency is associated with epididymis dysplasia and impaired sperm fertilization potential in the mouse. *Mol Rep Devel*. **85**(8–9):682–695.

Koju NP, He K, Chalise MK, Ray C, Chen Z, Zhang B, Wan T, Chen S, Jiang X. 2017. Multilocus approaches reveal underestimated species diversity and inter-specific gene flow in pikas (*Ochotona*) from southwestern China. *Mol Phylogenet Evol*. **107**:239–245.

Kottler EJ, Dickman EE, Sexton JP, Emery NC, Franks SJ. 2021. Draining the swamping hypothesis: little evidence that gene flow reduces fitness at range edges. *Trends Ecol Evol*. **36**(6):533–544.

Kuhlwilm M, Gronau I, Hubisz MJ, de Filippo C, Prado-Martinez J, Kircher M, Fu Q, Burbano HA, Lalueza-Fox C, de la Rasilla M, *et al.* 2016. Ancient gene flow from early modern humans into Eastern Neanderthals. *Nature*. **530**(7591):429–433.

Kyogoku D, Kokko H. 2020. Species coexist more easily if reinforcement is based on habitat preferences than on species recognition. *J Anim Ecol*. **89**(11):2605–2616.

Labroo MR, Studer AJ, Rutkoski JE. 2021. Heterosis and hybrid crop breeding: a multidisciplinary review. *Front Genet*. **12**:643761.

Lambert SM, Streicher JW, Fisher-Reid MC, Méndez de la Cruz FR, Martínez-Méndez N, García-Vázquez UO, Nieto Montes de Oca A, Wiens JJ. 2019. Inferring introgression using RADseq and DFOIL: power and pitfalls revealed in a case study of spiny lizards (Sceloporus). *Mol Ecol Resour*. **19**(4):818–837.

Lanfear R, Frandsen PB, Wright AM, Senfeld T, Calcott B. 2017. Partitionfinder 2: new methods for selecting partitioned models of evolution for molecular and morphological phylogenetic analyses. *Mol Phylogenet Evol*. **34**(3):772–773.

Lanier HC, Massatti R, He Q, Olson LE, Knowles LL. 2015. Colonization from divergent ancestors: glaciation signatures on contemporary patterns of genomic variation in collared pikas (*Ochotona collaris*). *Mol Ecol*. **24**(14):3688–3705.

Lawson DJ, van Dorp L, Falush D. 2018. A tutorial on how not to over-interpret STRUCTURE and ADMIXTURE bar plots. *Nat Commun*. **9**(1):3258.

Lefort V, Desper R, Gascuel O. 2015. FastME 2.0: a comprehensive, accurate, and fast distance-based phylogeny inference program. *Mol Biol Evol*. **32**(10):2798–2800.

Legras JL, Galeote V, Bigey F, Camarasa C, Marsit S, Nidelet T, Sanchez I, Couloux A, Guy J, Franco-Duarte R, *et al.* 2018. Adaptation of *S. cerevisiae* to fermented food environments reveals remarkable genome plasticity and the footprints of domestication. *Mol Biol Evol*. **35**(7):1712–1727.

Li H. 2011. A statistical framework for SNP calling, mutation discovery, association mapping and population genetical parameter estimation from sequencing data. *Bioinformatics*. **27**(21):2987–2993.

Li H, Durbin R. 2009. Fast and accurate short read alignment with Burrows–Wheeler transform. *Bioinformatics*. **25**(14):1754–1760.

Li H, Durbin R. 2011. Inference of human population history from individual whole-genome sequences. *Nature*. **475**(7357):493–496.

Li H, Handsaker B, Wysoker A, Fennell T, Ruan J, Homer N, Marth G, Abecasis G, Durbin R, Proc GPD. 2009. The sequence alignment/-map format and SAMtools. *Bioinformatics*. **25**(16):2078–2079.

Li D, Liu CM, Luo R, Sadakane K, Lam TW. 2015. MEGAHIT: an ultra-fast single-node solution for large and complex metagenomics assembly via succinct de Bruijn graph. *Bioinformatics*. **31**(10): 1674–1676.

Lissovsky AA. 2016. Class Mammalia. Order Lagomorpha. Family Ochotonidae (pikas). In: Wilson DE, Mittermeier RA, Lacher TE, editors. *Handbook of the mammals of the world, 6. Lagomorphs and rodents 1*. Barcelona: Lynx Edicions. p. 28–60.

Lissovsky AA, Yatsentyuk SP, Koju NP. 2019. Multilocus phylogeny and taxonomy of pikas of the subgenus *Ochotona* (Lagomorpha, Ochotonidae). *Zool Scri*. **48**(1):1–16.

Litsios G, Salamin N. 2014. Hybridisation and diversification in the adaptive radiation of clownfishes. *BMC Evol Biol*. **14**(1):245.

Liu SY, Jin W, Liao R, Sun ZY, Zeng T, Fu JR, Liu Y, Wang X, Li PF, Tang MK, *et al*. 2017. Phylogenetic study of *Ochotona* based on mitochondrial Cytb and morphology with a description of one new subgenus and five new species. *Acta Theriol Sinica*. **37**(1):1–43.

Liu KJ, Steinberg E, Yozzo A, Song Y, Kohn MH, Nakhleh L. 2015. Interspecific introgressive origin of genomic diversity in the house mouse. *Proc Natl Acad Sci U S A*. **112**(1):196–201.

Malhi Y, Doughty CE, Galetti M, Smith FA, Svenning JC, Terborgh JW. 2016. Megafauna and ecosystem function from the Pleistocene to the Anthropocene. *Proc Natl Acad Sci U S A*. **113**(4):838–846.

Malinsky M, Matschiner M, Svardal H. 2021. Dsuite – fast D-statistics and related admixture evidence from VCF files. *Mol Ecol Resour*. **21**(2):584–595.

Malinsky M, Svardal H, Tyers AM, Miska EA, Genner MJ, Turner GF, Durbin R. 2018. Whole-genome sequences of Malawi cichlids reveal multiple radiations interconnected by gene flow. *Nat Ecol Evol*. **2**(12):1940–1955.

Malinsky M, Trucchi E, Lawson D J, Falush D. 2018. RADpainter and fineRADstructure: population inference from RADseq Data. *Mol Biol Evol*. **35**:1284–1290.

Mark K, Barton NH. 1997. Evolution of a species' range. *Am Nat*. **150**(1):1–23.

Martin SH, Belleghem SMV. 2017. Exploring evolutionary relationships across the genome using topology weighting. *Genetics*. **206**(1):429–438.

Matute DR. 2010. Reinforcement can overcome gene flow during speciation in *Drosophila*. *Curr Biol*. **20**(24):2229–2233.

Melo-Ferreira J, Alves PC. 2018. Systematics of lagomorphs. In: Smith A, Johnston CH, Alves PC, Hacklaender K, editors. *Lagomorphs: pikas, rabbits, and hares of the world*. Baltimore: Johns Hopkins University Press. p. 3–12.

Mobley KB, Granroth-Wilding H, Ellmen M, Vähä JP, Aykanat T, Johnston SE, Orell P, Erkinaro J, Primmer CR. 2019. Home ground advantage: local Atlantic salmon have higher reproductive fitness than dispersers in the wild. *Sci Adv*. **5**(2):eaav1112.

Moerman F, Fronhofer EA, Wagner A, Altermatt F. 2020. Gene swamping alters evolution during range expansions in the protist *Tetrahymena thermophila*. *Biol Lett*. **16**(6):20200244.

Moran BM, Payne C, Langdon Q, Powell DL, Brandvain Y, Schumer M. 2021. The genomic consequences of hybridization. *Elife*. **10**: e69016.

Moyle LC, Nakazato T. 2010. Hybrid incompatibility "snowballs" between Solanum species. *Science*. **329**(5998):1521–1523.

Muscarella R, Galante PJ, Soley-Guardia M, Boria RA, Kass JM, Uriarte M, Anderson RP. 2014. ENMeval: an R package for conducting spatially independent evaluations and estimating optimal model complexity for MAXENT ecological niche models. *Methods Ecol Evol*. **5**(11):1198–1205.

Myers EA, Mulcahy DG, Falk B, Johnson K, Carbi M, de Queiroz K. 2021. Interspecific gene flow and mitochondrial genome capture during the radiation of Jamaican anolis lizards (Squamata; Iguanidae). *Syst Biol*. **73**(1):501–511.

Nakamura T, Yamada KD, Tomii K, Katoh K. 2018. Parallelization of MAFFT for large-scale multiple sequence alignments. *Bioinformatics*. **34**(14):2490–2492.

Nguyen LT, Schmidt HA, von Haeseler A, Minh BQ. 2015. IQ-TREE: a fast and effective stochastic algorithm for estimating maximum-likelihood phylogenies. *Mol Phylogenet Evol*. **32**(1):268–274.

Niu Y, Wei F, Li M, Liu X, Feng Z. 2004. Phylogeny of pikas (Lagomorpha, *Ochotona*) inferred from mitochondrial cytochrome b sequences. *Folia Zoologica*. **53**:141–155.

Owens GL, Samuk K. 2020. Adaptive introgression during environmental change can weaken reproductive isolation. *Nat Clim Chang*. **10**(1):58–62.

Pan YW, Zhang C, Lu Y, Ning ZL, Lu DS, Gao Y, Zhao XH, Yang YJ, Guan YQ, Mamatyusupu D, *et al*. 2022. Genomic diversity and post-admixture adaptation in the Uyghurs. *Nat Sci Rev*. **9**:3.

Panneerdoss S, Siva AB, Kameshwari DB, Rangaraj N, Shivaji S. 2012. Association of lactate, intracellular ph, and intracellular calcium during capacitation and acrosome reaction: contribution of hamster sperm dihydrolipoamide dehydrogenase, the E3 subunit of pyruvate dehydrogenase complex. *J Androl*. **33**(4):699–710.

Papadopulos AST, Igea J, Smith TP, Hutton I, Baker WJ, Butlin RK, Savolainen V. 2019. Ecological speciation in sympatric palms: 4. Demographic analyses support speciation of Howea in the face of high gene flow. *Evolution*. **73**(9):1996–2002.

Patterson N, Moorjani P, Luo YT, Mallick S, Rohland N, Zhan YP, Genschoreck T, Webster T, Reich D. 2012. Ancient admixture in human history. *Genetics*. **192**(3):1065.

Pickrell JK, Pritchard JK. 2012. Inference of population splits and mixtures from genome-wide allele frequency data. *PLOS Gen*. **8**(11): e1002967.

Price MN, Dehal PS, Arkin AP. 2010. Fasttree 2 – approximately maximum-likelihood trees for large alignments. *PLoS ONE*. **5**(3): e9490.

Pritchard JK, Stephens M, Donnelly P. 2000. Inference of population structure using multilocus genotype data. *Genetics*. **155**(2):945–959.

Pulido-Santacruz P, Aleixo A, Weir JT. 2020. Genomic data reveal a protracted window of introgression during the diversification of a neotropical woodcreeper radiation. *Evolution*. **74**(5):842–858.

Purcell S, Neale B, Todd-Brown K, Thomas L, Ferreira MAR, Bender D, Maller J, Sklar P, de Bakker PIW, Daly MJ, *et al*. 2007. PLINK: a tool set for whole-genome association and population-based linkage analyses. *Am J Hum Genet*. **81**(3):559–575.

Quilodran C, Montoya-Burgos J, Currat M. 2020. Harmonizing hybridization dissonance in conservation. *Commun Biol*. **3**:391.

Ralls K, Ballou JD, Dudash MR, Eldridge MDB, Fenster CB, Lacy RC, Sunnucks P, Frankham R. 2018. Call for a paradigm shift in the genetic management of fragmented populations. *Conserv Lett*. **11**(2):e12412.

Ralls K, Sunnucks P, Lacy RC, Frankham R. 2020. Genetic rescue: a critique of the evidence supports maximizing genetic diversity rather than minimizing the introduction of putatively harmful genetic variation. *Biol Conserv*. **251**:108784.

Rambaut A. 2010. *Figtree v1.40. Institute of evolutionary biology*. Edinburgh: University of Edinburgh. http://tree.bio.ed.ac.uk/software/figtree/.

Robinson ZL, Bell DA, Dhendup T, Luikart G, Whiteley AR, Kardos M. 2021. Evaluating the outcomes of genetic rescue attempts. *Conserv Biol*. **35**(2):666–677.

Rohlf FJ. 2005. *Tpsdig, digitize landmarks and outlines, version 2.05*: Department of Ecology and Evolution, State University of New York at Stony Brook. http://www.sbmorphometrics.org/soft-dataacq.html

Ronquist F, Teslenko M, van der Mark P, Ayres DL, Darling A, Hohna S, Larget B, Liu L, Suchard MA, Huelsenbeck JP. 2012. Mrbayes 3.2: efficient Bayesian phylogenetic inference and model choice across a large model space. *Syst Biol*. **61**(3):539–542.

Rosenberg NA, Pritchard JK, Weber JL, Cann HM, Kidd KK, Zhivotovsky LA, Feldman MW. 2002. Genetic structure of human populations. *Science*. **298**(5602):2381–2385.

Scherz MD, Masonick P, Meyer A, Hulsey CD. 2022. Between a rock and a hard polytomy: phylogenomics of the rock-dwelling *Mbuna* Cichlids of Lake Malaŵi. *Syst Biol*. **71**:741–757.

Schmieder R, Edwards R. 2011. Quality control and preprocessing of metagenomic datasets. *Bioinformatics*. **27**(6):863–864.

Seddon AW, Macias-Fauria M, Long PR, Benz D, Willis KJ. 2016. Sensitivity of global terrestrial ecosystems to climate variability. *Nature*. **531**(7593):229–232.

Servedio MR, Noor MAF. 2003. The role of reinforcement in speciation: theory and data. *Annu Rev Ecol Evol Syst*. **34**(1):339–364.

Shaw KL. 2002. Conflict between nuclear and mitochondrial DNA phylogenies of a recent species radiation: what mtDNA reveals and conceals about modes of speciation in Hawaiian crickets. *Proc Natl Acad Sci U S A*. **99**(25):16122–16127.

Shirsekar G, Devos J, Latorre SM, Blaha A, Dias MQ, Hernando AG, Lundberg DS, Burbano HA, Fenster CB, Weigel D. 2021. Multiple sources of introduction of North American *Arabidopsis thaliana* from across Eurasia. *Mol Biol Evol*. **38**(12):5328–5344.

Simão FA, Waterhouse RM, Ioannidis P, Kriventseva EV, Zdobnov EM. 2015. BUSCO: assessing genome assembly and annotation completeness with single-copy orthologs. *Bioinformatics*. **31**(19):3210–3212.

Sjodin BMF, Galbreath KE, Lanier HC, Russello MA. 2021. Chromosome-level reference genome assembly for the American pika (*Ochotona princeps*). *J Hered*. **112**(6):549–557.

Smith AB, Beever EA, Kessler AE, Johnston AN, Ray C, Epps CW, Lanier HC, Klinger RC, Rodhouse TJ, Varner J, *et al*. 2019. Alternatives to genetic affinity as a context for within-species response to climate. *Nat Clim Chang*. **9**(10):787–794.

Smith AT, Foggin JM. 1999. The plateau pika (*Ochotona curzoniae*) is a keystone species for biodiversity on the Tibetan plateau. *Anim Conserv*. **2**(4):235–240.

Smith A, Johnston CH, Alves PC, Hacklaender K, Smith A, Johnston CH, Alves PC, Hacklaender K. 2018. *Lagomorphs: pikas, rabbits, and hares of the world*. Baltimore: Johns Hopkins University Press.

Stamatakis A. 2014. RAxML version 8: a tool for phylogenetic analysis and post-analysis of large phylogenies. *Bioinformatics*. **30**:1312–1313.

Stelkens RB, Brockhurst MA, Hurst GD, Greig D. 2014. Hybridization facilitates evolutionary rescue. *Evol Appl*. **7**(10):1209–1217.

Sumbh O, Hof AR. 2022. Can pika hold the umbrella? Understanding the current and future umbrella potential of keystone species Pika (*Ochotona* sp.). *Glob Eco Conserv*. **38**(2022):e02247.

Talavera G, Castresana J. 2007. Improvement of phylogenies after removing divergent and ambiguously aligned blocks from protein sequence alignments. *Syst Biol*. **56**(4):564–577.

Teng HJ, Zhang YH, Shi CM, Mao FB, Cai WS, Lu L, Zhao FQ, Sun ZS, Zhang JX. 2017. Population genomics reveals speciation and introgression between brown Norway rats and their sibling species. *Mol Biol Evol*. **34**(9):2214–2228.

Terhorst J, Kamm JA, Song YS. 2017. Robust and scalable inference of population history from hundreds of unphased whole genomes. *Nat Gen*. **49**(2):303–309.

Theobald D M, Kennedy C, Chen B, Oakleaf J, Baruch-Mordo S, Kiesecker J. 2020. Earth transformed: detailed mapping of global human modification from 1990 to 2017. *Earth Syst Sci Data***12**: 1953–1972.

Vuillaume B, Valette V, Lepais O, Grandjean F, Breuil M. 2015. Genetic evidence of hybridization between the endangered native species *Iguana delicatissima* and the invasive *Iguana iguana* (Reptilia, Iguanidae) in the lesser antilles: management implications. *PLoS One*. **10**(6):e0127575–e0127575.

Waller DM. 2015. Genetic rescue: a safe or risky bet? *Mol Ecol*. **24**(11): 2595–2597.

Wan XR, Zhang ZB. 2017. Climate warming and humans played different roles in triggering Late Quaternary extinctions in east and west Eurasia. *P Roy Soc B-Biol Sci*. **284**:1851.

Wang P, Burley JT, Liu Y, Chang J, Chen D, Lu Q, Li SH, Zhou X, Edwards S, Zhang Z. 2020. Genomic consequences of long-term population decline in brown eared pheasant. *Mol Phylogenet Evol*. **38**(1):263–273.

Wang XY, Liang D, Jin W, Tang MK, Shalayiwu LS, Zhang P. 2020. Out of Tibet: genomic perspectives on the evolutionary history of extant pikas. *Mol Biol Evol*. **37**(6):1577–1592.

Weeks AR, Heinze D, Perrin L, Stoklosa J, Hoffmann AA, van Rooyen A, Kelly T, Mansergh I. 2017. Genetic rescue increases fitness and aids rapid recovery of an endangered marsupial population. *Nat Commun*. **8**(1):1071.

Wen ZX, Yang QS, Quan Q, Xia L, Ge DY, Lv X. 2016. Multiscale partitioning of small mammal β-diversity provides novel insights into the Quaternary faunal history of Qinghai–Tibetan Plateau and Hengduan Mountains. *J Biogeogr*. **43**(7):1412–1424.

Whiteley AR, Fitzpatrick SW, Funk WC, Tallmon DA. 2015. Genetic rescue to the rescue. *Trends Ecol Evol*. **30**(1):42–49.

Wickham H. 2016. *Ggplot2: elegant graphics for data analysis*. New York: Springer-Verlag.

Wilson MC, Smith AT. 2015. The pika and the watershed: the impact of small mammal poisoning on the ecohydrology of the Qinghai–Tibetan Plateau. *Ambio*. **44**(1):16–22.

Wolf JBW, Ellegren H. 2017. Making sense of genomic islands of differentiation in light of speciation. *Nat Rev Genet*. **18**(2):87–100.

Wu SD, Wang Y, Wang ZF, Shrestha N, Liu JQ. 2022. Species divergence with gene flow and hybrid speciation on the Qinghai–Tibet Plateau. *New Phytol* **234**(2):392–404.

Yang SJ, Dong HL, Lei FM. 2009. Phylogeography of regional fauna on the Tibetan Plateau: a review. *Prog Nat Sci*. **19**(7):789–799.

Zdobnov EM, Kuznetsov D, Tegenfeldt F, Manni M, Berkeley M, Kriventseva EV. 2020. OrthoDB in 2020: evolutionary and functional annotations of orthologs. *Nucleic Acids Res*. **49**(D1):D389–D393.

Zeng L, Ming C, Li Y, Su LY, Su YH, Otecko NO, Dalecky A, Donnellan S, Aplin K, Liu XH, *et al*. 2018. Out of southern East Asia of the brown rat revealed by large-scale genome sequencing. *Mol Biol Evol*. **35**(1):149–158.

Zhang C, Rabiee M, Sayyari E, Mirarab S. 2018. ASTRAL-III: polynomial time species tree reconstruction from partially resolved gene trees. *BMC Bioinform*. **19**(6):153.

Zhang DZ, Tang L, Cheng YL, Hao Y, Xiong Y, Song G, Qu YH, Rheindt FE, Alstrom P, Jia CX, *et al*. 2019. 'Ghost introgression' as a cause of deep mitochondrial divergence in a bird species complex. *Mol Biol Evol*. **36**(11):2375–2386.

Zhao Y, Tzedakis PC, Li Q, Qin F, Cui QY, Liang C, Birks HJB, Liu YL, Zhang ZY, Ge JY, *et al*. 2020. Evolution of vegetation and climate variability on the Tibetan Plateau over the past 1.74 million years. *Sci Adv*. **6**(19):eaay6193.

Zheng YC, Janke A. 2018. Gene flow analysis method, the D-statistic, is robust in a wide parameter space. *BMC Bioinform*. **19**:10.